DOE/MC/27225--3258

DE93 008552

BIOLOGICAL CONVERSION OF SYNTHESIS GAS

Topical Report: Mass Transfer/Kinetic Studies

by

K. T. Klasson
R. Basu
E. R. Johnson
E. C. Clausen
J. L. Gaddy

March 1992

Work performed under Grant No. DE-FG21-90MC27225

for

U. S. Department of Energy
Morgantown Energy Technology Center
Morgantown, West Virginia

by

University of Arkansas
Fayetteville, Arkansas

ACKNOWLEDGMENT

Financial support for this work has been provided by the Morgantown Energy Technology Center, U. S. Department of Energy under grant number DE-FG21-90MC27225.

TABLE OF CONTENTS

LIST OF TABLES

LIST OF TABLES

LIST OF FIGURES

LIST OF FIGURES - continued

1.0 INTRODUCTION

Synthesis gas, a mixture of primarily CO, H_2 and CO_2, is a major building block in the production of fuels and chemicals. The gas is derived from non-gaseous raw materials such as coal, shale oil, tar sands, heavy residue and biomass. The composition of synthesis gas is dependent upon the raw material used and the gasification process. Coal-derived gas is rich in CO and H_2, with lower concentrations of CO_2 and CH_4 and traces of H_2S and COS (1).

Synthesis gas may be used in the production of both gaseous and liquid fuels. The conventional method of producing gaseous fuel first employs the catalytic shift reaction. In this reaction, CO and H_2O are converted into H_2 and CO_2. Following the removal of excess CO_2 and sulfur contaminants such as H_2S and COS, the H_2 and CO_2 are catalytically methanated to CH_4 and H_2O. After drying, the product gas contains 95-98% CH_4.

Most methanation processes require temperatures of 300-700°C and operating pressures of 3-20 atm (2). The catalysts used for the methanation step include nickel and potassium-based catalysts, as well as mixtures of iron/chromium oxides and zinc/copper oxides (3,4). Poisons for these catalysts include chlorine and sulfur (5,6). In addition, chemical catalytic processes are known to produce by-products such as methanol, formaldehyde and acetic acid (7).

A wide variety of both liquid and gaseous fuels may be produced from synthesis gas using Fischer-Tropsch synthesis including light hydrocarbons (methane, ethane), fuel range hydrocarbon distillates and heavy waxes. The stoichiometry for product formation may be ideally represented by the equation:

$$CO + 2\ H_2 \rightarrow (-CH_2-) + H_2O \quad (1.1)$$

However, based on actual yields in a Synthol entrained flow reactor, the overall stoichiometry is better characterized by the empirical relation (8):

$$CO + 2.12\ H_2 \rightarrow (HC, Alcohols, Acids) + 0.95\ H_2O \quad (1.2)$$

As is noted in Equations (1.1) and (1.2), about 2 moles of H_2 are required for every mole of CO.

The H_2/CO ratio in synthesis gas is dependent upon both the grade of coal used in the feed and the type of gasifier employed. Modern gasifiers produce synthesis gas with a H_2/CO ratio as low as 0.6. Therefore, an increase in the H_2 content of synthesis gas is usually necessary prior to Fischer-Tropsch synthesis, which requires coupling water gas shift and gasification.

The utilization of coal to produce liquid fuels by Fischer-Tropsch synthesis is a multi-step process. After gasification at 700-2000°C (9), the raw gas is quenched and scrubbed to condense tars and oils and to remove dust and water soluble materials from the gas stream such as phenols, chloride, ammonia, cyanide, thiocyanate, and perhaps some H_2S (10). A catalytic water-gas shift conversion at about 225°C is then used to adjust the H_2/CO ratio:

$$CO + H_2O \rightarrow CO_2 + H_2 \quad (1.3)$$

A high H_2/CO ratio is not only necessary to satisfy the stoichiometry of the Fischer-Tropsch synthesis, but is beneficial in controlling carbon deposition and reducing associated catalyst deactivation (11).

Following shift conversion, the gas contains primarily H_2, CO, CO_2, H_2O, sulfur gases and possibly methane, although small amounts of higher aliphatic hydrocarbons and light oils are sometimes present. The sulfur is present as H_2S ad COS, with smaller amounts of organic sulfides or mercaptans. These "acid gases", including CO_2, are removed using a variety of processes,

including Claus, absorption, or liquid phase oxidation processes. The sulfur concentration must be reduced to less than 0.1 ppm to protect sensitive downstream catalysts (10). Following purification, the gas is then available for conversion to C_1-C_{35} hydrocarbons in a Fischer-Tropsch synthesis reactor at 225-365°C.

There are several limitations with water gas shift, purification and Fischer-Tropsch synthesis. Each of these operations are conducted in separate steps, at different conditions requiring intermediate adjustment of temperature or pressure, which results in a very complex and expensive process. Also, these processes are carried out at elevated temperatures and pressures, and thus suffer from low thermal efficiencies. The catalysts used in the Fischer-Tropsch synthesis are particularly sensitive to the presence of sulfur gases or carbon deposition and deteriorate rapidly. Carbon deposition, as was mentioned previously, is enhanced by low H_2/CO ratios in the synthesis gas. Finally, more specific catalysts are required to avoid production of a broad array of chemicals and fuels and to improve raw material yields from Fischer-Tropsch synthesis.

1.1 Biological Synthesis Gas Conversion

Biological processes may be utilized as an alternative to the traditional methods of producing fuels from raw synthesis gas. Biological processes operate at near ambient temperatures, and yields and energy efficiencies are high. Many microorganisms (biocatalysts) are not sensitive to the presence of low concentrations of toxic gas compounds found in synthesis gas (12,13). In addition, biological reactions are very specific, and often a single product is produced as a result of biosynthesis.

A single reaction vessel can often be used to carry out several biological reactions in series or parallel. Therefore, one reactor might be used for water gas shift, gas purification (sulfur and CO_2 removal) and product formation (Fischer-Tropsch synthesis or methanation) by utilizing a co-culture or mixed culture. As is shown in Figure 1.1, the process for biological production of hydrocarbons from synthesis gas could be very simple. Following gasification, the gas temperature would be reduced to 95-135°F, with the opportunity for heat recovery and improved energy efficiency. The cool gases would then be bubbled through a biological reactor, where a culture of microorganisms would be maintained to produce H_2 and remove sulfur gases and CO_2. Cultures may be developed that utilize CO, CO_2 and H_2 as substrates to produce hydrocarbons, such that adjustment of the H_2/CO ratio in the synthesis gas is not essential. Also, the removal of CO_2 may not be necessary if a liquid product is produced in the reactor. High conversions in the reactor will be necessary to avoid recycle. Therefore, significant potential exists for developing a simple, more economical biological process for hydrocarbon production from coal.

The disadvantages of biological processes include slower reactions and the need for sterile conditions to prevent contamination. When utilizing synthesis gas, sterility is insured by the presence of CO, which is toxic to most microorganisms. Biological reactions involving gaseous substrates may be operated under mass transfer limiting conditions, where mass transfer controls the rate of transport of gaseous reactants and, consequently, reactor size. Reactor rates have been found to be proportional to pressure, and the use of special bioreactors at moderate pressures (150 psia) have resulted in residence times for near complete conversion of synthesis gas of only a few

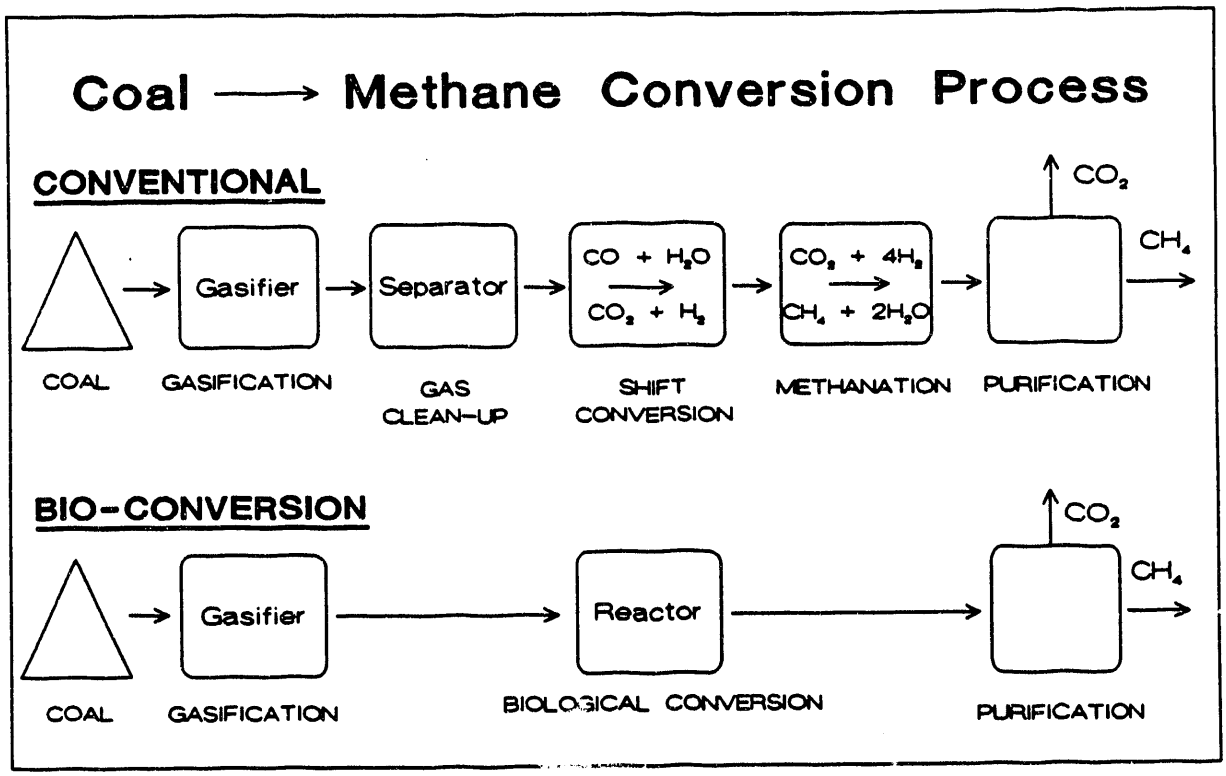

Figure 1.1. Comparison of Conventional and biological routes for methane production from coal.

minutes (14,15). Therefore, fast reaction rates and small reactors can be achieved by the appropriate bioreactor design.

1.2 Brief Statement of Purpose

The purpose of the proposed research is to develop a technically and economically feasible process for biologically producing H_2 from synthesis gas while, at the same time, removing harmful sulfur gas compounds. This research builds upon previous research studies carried out in the University of Arkansas laboratories where the technical and economic feasibility of biologically producing CH_4 from synthesis gas components has been demonstrated. Six major tasks are being studied:

1. Culture development, where the best cultures are selected and conditions optimized for simultaneous hydrogen production and sulfur gas removal;

2. Mass transfer and kinetic studies in which equations necessary for process design are developed;

3. Bioreactor design studies, where the cultures chosen in Task 1 are utilized in continuous reaction vessels to demonstrate process feasibility and define operating conditions;

4. Evaluation of biological synthesis gas conversion under limiting conditions in preparation for industrial demonstration studies;

5. Process scale-up where laboratory data are scaled to larger-size units in preparation for process demonstration in a pilot-scale unit; and

6. Economic evaluation, where process simulations are used to project process economics and identify high cost areas during sensitivity analyses.

The bioconversion studies are built upon previous experimental work performed under DOE contract. A strong foundation in gaseous substrate

fermentation with a major emphasis on continuous bioreactor design and operation has been achieved. Although the technical feasibility of biological methane production from synthesis gas has been demonstrated, several important pieces of information are needed prior to recommending a demonstration unit for this biological conversion. These process development studies can be grouped into three catagories:

1. Culture development under industrial conditions;
2. Investigation of alternate reactor systems to minimize capital costs; and
3. Process scale-up measurements.

Culture development studies under industrial conditions involve operating the cultures under less than optimum conditions in order to define operating limits for the cultures. The effects of trace quantities of oxygen in the feed on the strict anaerobes will be quantified. In addition, synthesis gas contaminants other than sulfur gases will be added to the gas stream to measure the effects of these materials on cell growth, substrate consumption and product formation. The effects of various CO/H_2 ratios on product yield and fermentation rates will be measured. Finally, efforts will be directed toward developing a cheap minimal media for synthesis gas fermentation.

An economic evaluation of various reactor alternatives has shown that the use of traditional mass transfer equipment yields high capital costs due to relatively poor gas-liquid mass transfer. A reaction system with mass transfer capabilities that minimize capital costs is thus sought. Various reaction systems are potential candidates and will be tested, including modified trickle-bed reactors and pulse and airlift fermenters. Also, various compounds will be added to the fermentation media in an effort to increase the mass transfer coefficient by changing physical properties.

Scale-up measurements involve several experiments. First, physical properties of the fermentation media will be evaluated under a variety of fermentation conditions. Two physical properties, medium viscosity and surface tension, are thought to change significantly with increasing cell density during the fermentation. Methods for handling these changes during process scale-up will be addressed. SEcondly, the limiting conditions of gas-liquid fermentation need to be defined. The maximum operable cell density and the performance of the cultures under extreme agitation rates, cell densities, operating pressure and high product concentrations will be evaluated. Finally, the scale-up correlations used in the economic analysis will be tested in larger bench-scale continuous reactors prior to recommending orocess demonstration in a PDU.

The production of hydrogen from CO and water can be carried out biologically by the facultative photosynthetic bacterium *Rhodospirillum rubrum* as an alternative to the water gas shift reaction. H_2 production is essentially in adjusting the H_2/CO ratio for further utilization of the syngas. Experiments in the University of Arkansas laboratories have shown that this bacterium is fast growing, exhibits fast CO uptake and is table in the presence of high CO and sulfur gas compositions. *R. rubrum* requires a tungsten light source for growth; however, the actual chemical reaction can be carried out in the dark. Therefore, only a small bioreactor for bacterial growth is required, thereby reducing capital and radiant energy costs.

Sulfur gas removal may be carried out by the anaerobic bacterium *Chlorobium thiosulfatophilum* (16,17). *C. thiosulfatophilum*, a phototropic sulfur bacterium, has the advantage of producing sulfur which could be easily

separated as a solid by-product. It has also been shown to utilize COS in conjunction with the chemical reaction

$$COS + H_2O \rightarrow CO_2 + H_2S \qquad (1.4)$$

on *C. thiosulfatophilum* is superior to other sulfur gas-utilizing species such as *Thiobacillus denitrificans*, which produces sulfate as the product in H_2S conversion (18,19).

1.2.1 Purpose

The purpose of this report is to present results from mass transfer and kinetic studies employing *R. rubrum* and *C. thiosulfatophilum*. Monod equations for growth using light as the limiting substrate are presented for both of the photosynthetic bacteria. Kinetic expressions for CO utilization by *R. rubrum* in producing H_2 by Equation (1.3) are presented as well as kinetic information for *C. thiosulfatophilum* in converting H_2S and COS to elemental sulfur.

2.0 MATERIALS AND METHODS

2.1 Organisms and Culture

Rhodospirillum rubrum, ATCC 25903, was obtained from the American Type Culture Collection, Rockville, MD. The medium used for stock cultures, transfers and experiments contained per 100 mL: Pfennig mineral solution (20), 5 mL; Pfennig trace metal solution (20) with the addition of 10 mg/l Na_2SeO_3 (21), 0.1 mL; B-vitamin solution (21), 0.5 mL; yeast extract (Difco), 0.1 g; $NaCH_3COO \cdot 3H_2O$, 0.58 g; NH_4Cl, 0.27 g; and $NaHCO_3$, 0.4 g. Stock cultures were kept anaerobically under tungsten light at 30°C and transferred every 2-3 weeks. Seed cultures used for inoculation of the bioreactors were prepared by transferring 5 mL of stock culture to 75 mL of fresh medium reduced with 1.5 mL of Na_2S (2.5%). Typically the seed culture was grown for 48 hours before an aliquot of 5 mL was used for inoculation of the reactor.

The medium for the studies with *C. thiosulfatophilum* contained per 100 mL: Phennig mineral solution (20), 5 mL; Pfennig trace metals solution (20), 0.1 mL; B-vitamins solution (21), 0.5 mL; yeast extract (Difco), 0.05 g; and $naHCO_3$, 0.4 g. Before sterilization, 75 mL of medium were added to each bottle under a N_2/CO_2 (80%20%) atmosphere. The bottles were autoclaved at 15 psig for 20 minutes. Once sterile, the bottles were flushed water He/CO_2 (60%/40%) to remove any traces of O_2 and inoculated with 5 mL of seed culture. Gaseous H_2S was then added to the bottles in the desired amounts. The seed culture was grown for 72 h before being used for inoculation into the bottles.

2.2 Batch Bioreactors and Operating Conditions

Batch fermentations were carried out in 150 mL glass serum bottles (Wheaton Glass Co., Millville, NJ). The bottles were sealed using butyl rubber septum stoppers and aluminum crimp seals (Bellco Glass Co., Vineland, NJ). Before sterilization, 75 mL of medium were added to each bottle under a He/CO_2 (75%/25%) atmosphere. The bottles were autoclaved at 15 psig for 20 minutes.

Once sterile, the bottles were reduced with 1.5 mL of Na_2S (2.5%) and inoculated with 5 mL of seed culture. After inoculation the desired gas phases were introduced by flushing with CO/CO_2 (80%/20%) for 3 minutes using an appropriate check valve to achieve the desired pressure. Argon (20 mL) was then added to each bottle as an inert tracer gas with a gas-tight syringe. This procedure allowed calculation of the amounts of each gas component through the fermentation.

The experiments were carried out in a modified incubator shaker (Model G25, New Brunswick Scientific Co., Edison, NJ) at 150 rpm and 30°C. Tungsten light, necessary for growth, was supplied in excess in the shaker.

The experiments involving light intensity were also carried out in a modified incubator shaker (Model G25, New Brunswick Scientific Co., Edison, NJ) at 150 rpm and 30°C. Tungsten light, necessary for growth, was supplied in the shaker. Each bottle was placed horizontally into a dark box, contained in the shaker incubator, with a light reduction filter (Kodak Wratten Gelatin Filter, Eastman Kodak Company, Rochester, NY) in the lid to control light intensity. Light intensities in the boxes were measured with a LX-101 Digital Lux Meter (Cole-Parmer, Chicago, IL).

2.3 Continuous Bioreactor and Operating Conditions

The continuous stirred-tank reactor used was a New Brunswick Scientific (Edison, NM) BioFlo II fermenter equipped with temperature, pH and agitation control. The liquid working volume was 1250 mL and the overhead gas volume was 350 mL. Illumination necessary for growth was supplied by two tungsten lights (40W) directed towards the glass fermentation jar. Experiments were carried out at 30°C and pH 7. The feed gas used was a mixture of H_2, Ar, CO and CO_2 (20/15/55/10%) and was continuously fed to the reactor. Liquid feed was also supplied on a continuous basis. A schematic of the equipment set-up is shown in Figure 2.1.

Typically experiments were started with constant agitation rate and gas flow rate. during an experimental run, the liquid flow rate was reduced from a high to low setting. This procedure induced an increase in cell concentration and CO conversion with time as the culture strived to reach a steady state for growth limited by medium composition, liquid flow rate and illumination. The conversion of CO was monitored and experiments were considered complete when the gas conversion leveled off. The liquid flow rate was then increased and the cell concentration allowed to decrease to a low level before starting a new experiment.

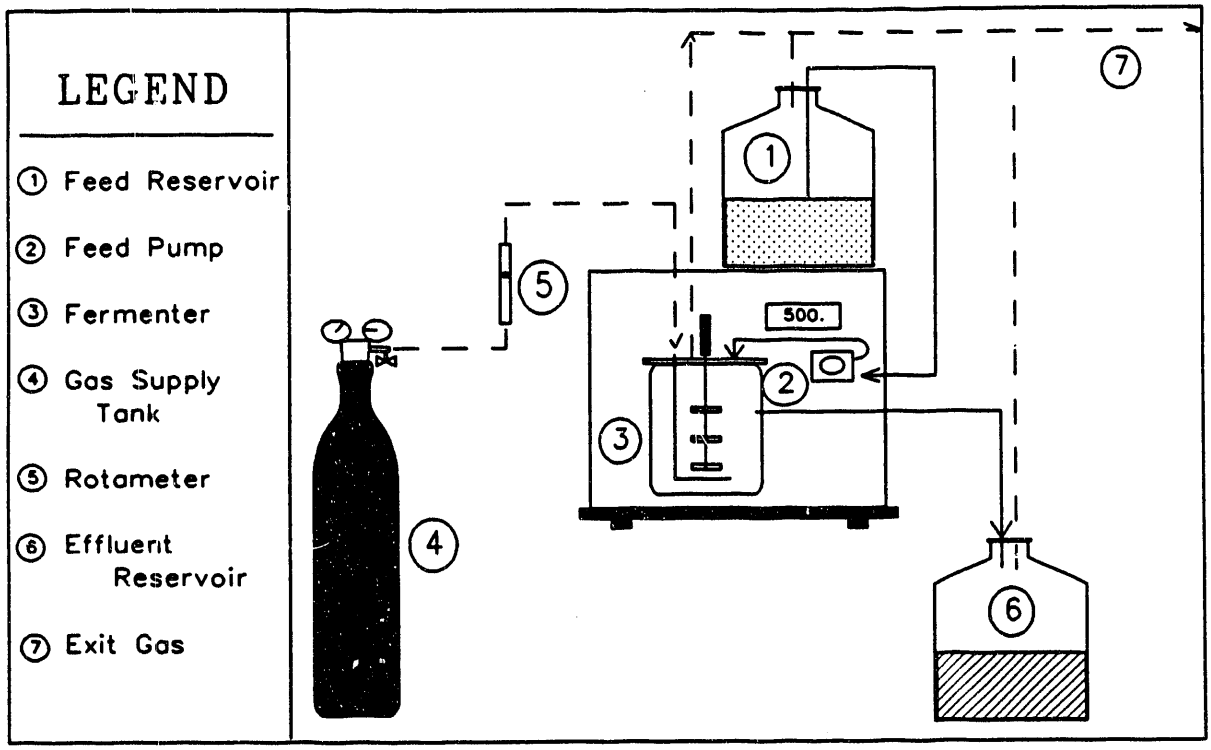

Figure 2.1. Schematic of the CSTR system using *R. rubrum*.. LEGEND: 1-Feed reservoir, 2-Feed pump, 3-Fermenter, 4-Gas supply tnak, 5-Rotameter, 6-Effluent reservoir, 7-Exit gas.

2.4 Analytical Techniques

Liquid and gas samples, 1.5 mL and 0.4 mL, respectively, were withdrawn from the reactors during the fermentation and analyzed for cell concentration and gas phase composition. The dry cell weight concentration for *R. rubrum* was obtained by measuring light scatter at 540 nm in a Spectronic 21 (Milton Roy Co., Rochester, NY) and converting it to cell density using a calibration curve (DCW(mg/l)) = 395.4•ABS_{540}). Cell concentration measurements for *C. thiosulfatophilum* are discussed later.

Gas analyses of CO, CO_2 and H_2 were performed on a gas chromatograph (Perkin-Elmer Sigma 300, Norwalk, CT) using an 1.8 m stainless steel column packed with Carbosphere, 60/80 mesh. The oven temperature was held constant at 135°C while the injector and thermal conductivity detector temperatures were 175°C. Helium was used as the carrier gas at a flow rate of 40 mL/min.

The gas phase H_2S concentrations were measured by gas chromatography using a Hewlett-Packard (Kennett Square, PA) HP 5890 Series II gas chromatograph and an HP 7673 integrator equipped with a thermal conductivity detector. The column was a 1/8" x 6' teflon column packed with Chromosorb 107, 80/100 mesh (Altech Assoc., Inc., Deerfield, IL). The oven temperature was 80°C, and the detector and injector temperatures were kept at 175°C. The carrier gas was helium at a flow rate of 30 mL/min. Liquid phase sulfur concentrations ($H_2S(l)$, HS^-, S^{2-}) were measured using a Corning Silver/Sulfide Electrode (Corning Glass Works, Medfield, MA) and an Orion Specific Ion meter (Orion Research, Inc., Cambridge, MA).

3.0 MASS TRANSFER/KINETIC CONCEPTS WITH RHODOSPIRILLACEAE

3.1 Specific Carbon Monoxide Uptake Rate for *R. rubrum*

In converting gaseous substrates by microorganisms present in a liquid phase, the gas must be transported from the bulk gas phase to the cell wall.

It is widely recognized (22) that the main resistance to this transport, for sparingly soluble gases such as CO and O_2, is the liquid film at the gas/liquid interface. All other transport phenomena are of lesser magnitude. The rate of transport then becomes proportional to the concentration driving force across the film. If the liquid phase concentration of CO is expressed in terms of partial pressure, Equation (3.1) may be written.

$$\text{Rate of transport} = \frac{K_L a}{H} (p_G - p_L^*) V_L \qquad (3.1)$$

In Equation (3.1), p_L^* is the partial pressure of CO in the gas phase which in equilibrium with the bulk liquid phase concentration of CO. For the sealed bioreactors used in this study, the rate of transport changes with time due to cell growth and consumption of CO by the cells. If the CO consumption rate in the liquid is very low, the driving force, $p_G - p_L^*$, is also small and the CO uptake rate is considered to be kinetically limited. On the other hand, if the reaction rate in the liquid is high and the CO is consumed as it enters the liquid, p_L^* approaches zero and the rate of uptake depends only upon the mass transfer rate. According to Equation (3.1), the rate of transport is then proportional to the partial pressure of CO in the gas phase times the liquid volume. In the unique case of gas consumption by a growing microbial culture, both of the rate limiting regions are present during the fermentation, given that the initial cell concentration is sufficiently low.

Since the solubility of CO in water (and medium) is low, it may be safely assumed that the amount of CO present in the liquid phase is negligible compared to the CO in the gas phase, n_{CO}. Thus, Equation (3.1) may be rewritten as:

$$\frac{1}{V_L}\left[\frac{dn_{CO}}{dt}\right] = \frac{K_L a}{H}\,(p_G - p_L^*) \qquad (3.2)$$

The disappearance of CO in the liquid phase due to microbial uptake may be expressed as proportional to the cell density in the liquid. The proportionality constant, q, is generally called the specific uptake rate and is defined in Equation (3.3).

$$\text{moles of CO consumed} = q \times V_L \qquad (3.3)$$

As for most microbial systems, the rate of substrate uptake by the cells, q, is dependent upon the availability of the substrate and thus the concentration of the dissolved gas becomes the primary variable. If the general assumption is made that substrate inhibition is present, Equation (3.4) may be used to describe the CO uptake per dry cell weight.

$$q = \frac{q_m p_L^*}{K_P + p_L + (p_L^*)^2/W} \qquad (3.4)$$

Equation (3.4) is the well known Monod model (23) rewritten for substrate uptake and modified by Andrews (24) to include substrate inhibition.

The determination of the parameters in Equation (3.4) is not straightforward since the partial pressure of CO in the liquid phase is difficult to measure. However, by using the data obtained late in the batch fermentation, the mass transfer coefficient, $K_L a$, may determined using Equation (3.2) and the assumption that p_L^* is zero. This value of $K_L a$ may then be used to calculate p_L^* for the part of the batch fermentation which is not under mass transfer limiting conditions. A simple stepwise procedure may be formulated for the determination of the parameters $K_L a$, q_m, K_p and W as follows.

1. Determine q from the experimental data and Equation (3.3) for the entire fermentation.

2. Determine K_La from the experimental data during the latter part of the fermentation using Equation (3.2) and the assumption that p_L^* is equal to zero.

3. Calculate p_L^* in the early part of the fermentation using the value of K_La found in Step 2 and Equation (3.2).

4. Rearranage Equation (3.4) to form Equation (3.5) so that the parameters are easily determined by plotting p_L^*/q as a function of p_L^* using a second order equation to the fit data by the method of least squares.

$$\frac{p_L^*}{q} = \frac{K_p}{q_m} + \frac{p_L^*}{q_m} + \frac{(p_L^*)^2}{q_m W} \qquad (3.5)$$

This technique has previously been demonstrated in detail by Vega *et al.* (25) for the fermentation of CO to acetate by *P. productus*.

Two sets of experiments (Experiments 1 and 2) were conducted with different initial CO partial pressures. By conducting two experiments, the reproducability of the experimental and analytical techniques was verified and a model covering a rather wide range of CO partial pressures was developed. In addition to the experiments with CO, a third experiment was conducted with various gas phase compositions (see Table 3.1) in a medium containing no acetate and 0.06% yeast extract. No H_2 production was observed in the bottles without CO, but cell growth remained essentially constant for all gas phase compositions. This result helps to verify that CO is utilized in H_2 production but is not utilized for cell growth.

The increase in cell concentration (Experiments 1 and 2) with time within each experiment was identical for all CO pressures studied (see Figure 3.1). However, the cell concentration profiles varied between experiments due to a

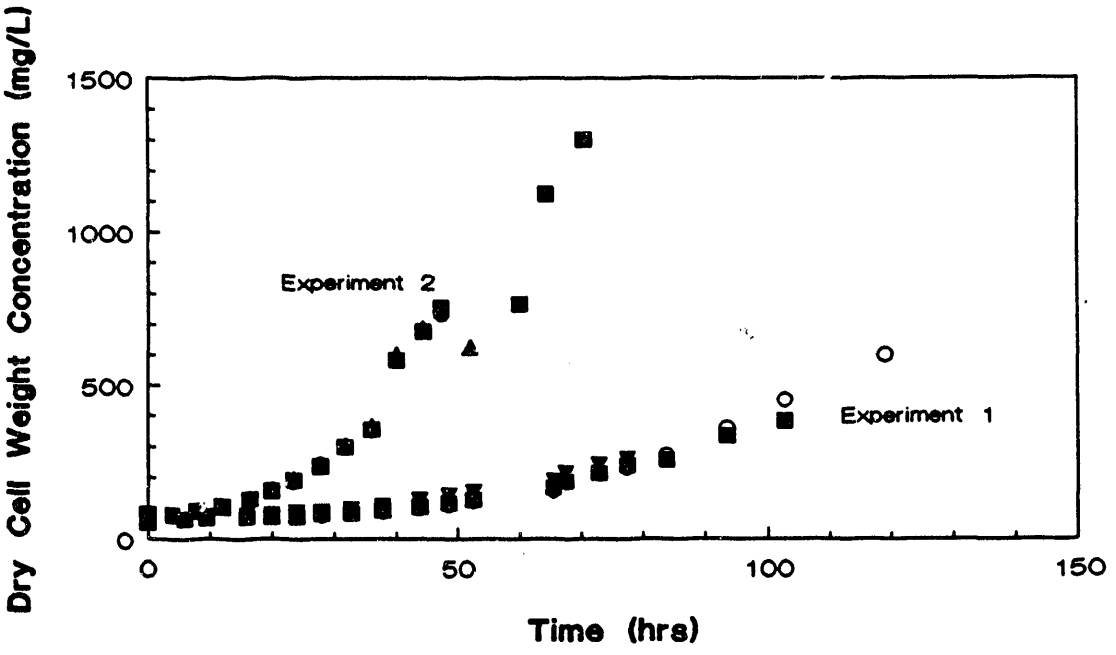

Figure 3.1. Cell concentration profiles in Experiments 1 and 2.

Table 3.1

Experiment 3 - effect of gas phase composition on cell growth and hydrogen production (inoculum size = 16 mg/l.)

Gas Phase Composition (mol percent)	Maximum Cell Concentration, 86 hr (mg/l)	Hydrogen Production
CO_2/He (25%/75%	209	-
CO_2/N_2 (25%/75%)	206	-
CO_2/CO (25%/75%)	208	++
CO_2/CO (50%/50%)	214	+
$CO_2/He/N_2$ (33%/34%/33%)	202	-

longer lag phase in one of the experiments. The differences in lag phase between the experiments may be caused by different inoculum histories. The CO was completely consumed by *R. rubrum* in both experiments (see Figures 3.2 and 3.3), with fermentation times for complete conversion ranging from 40 to 120 hours. The solid curves in Figures 3.2 and 3.3 correspond to the smooth curves used when estimating derivatives which were needed for the calculations of the CO uptake rate in Equation (3.2). As the CO was consumed, H_2 was produced in nearly stoichiometric amounts. The H_2 production with time is shown in Figures 3.4 and 3.5. As is seen, the reactor with the highest initial CO pressure produced the most H_2. The dashed curves in Figures 3.3 and 3.4 have only been added to emphasize trends in the raw data. A H_2 yield on CO of 0.87 mol/mol was found by examining all of the collected data (see Figure 3.6). This corresponds to 87% of the theoretical yield from Equation

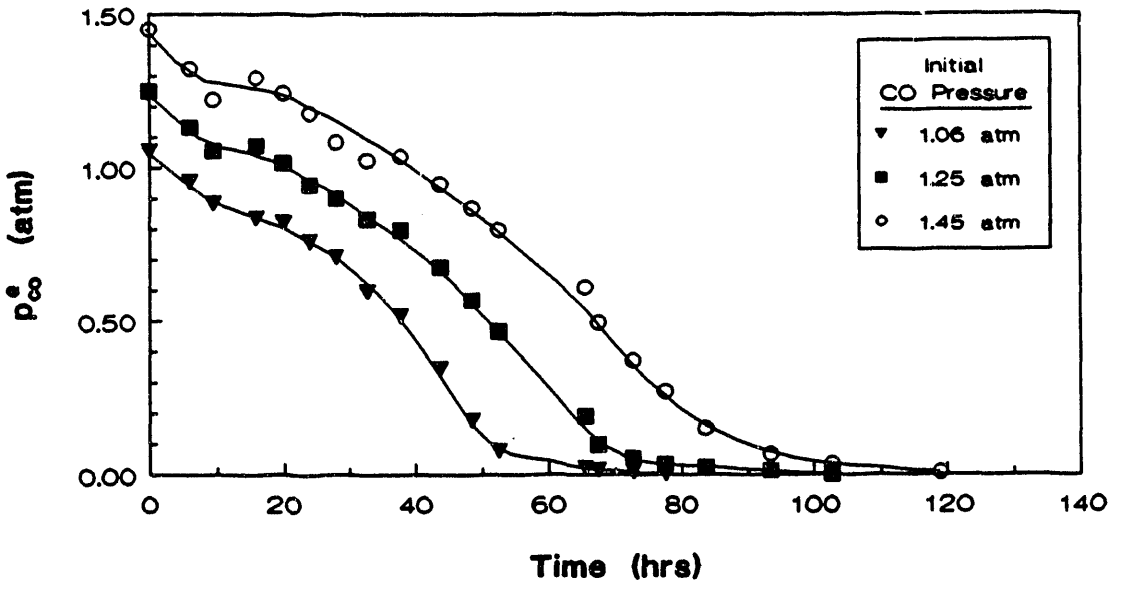

Figure 3.2. CO partial pressure profiles for *R. rubrum* in Experiment 1.

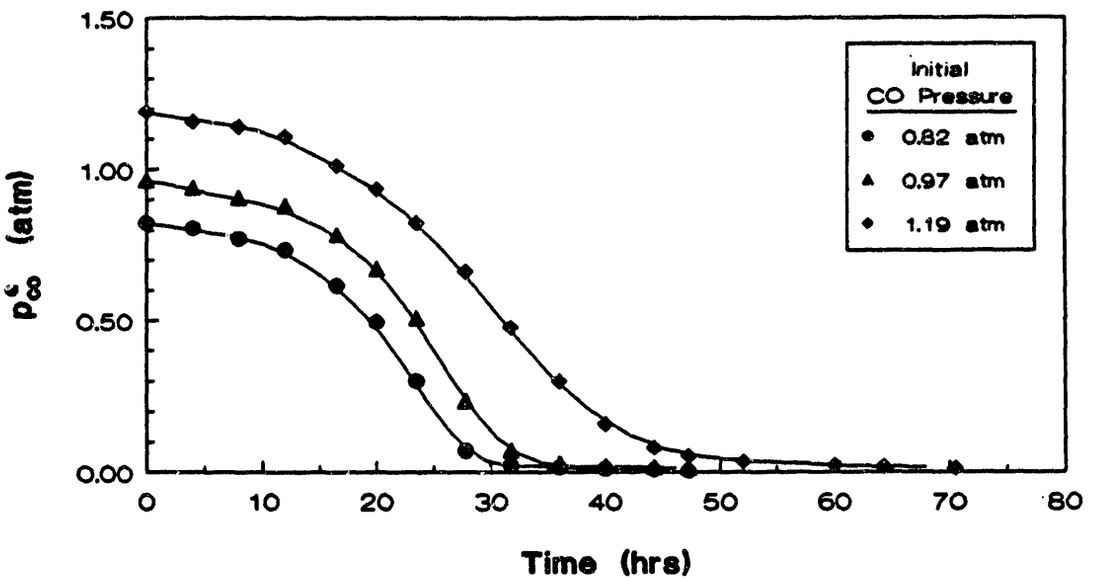

Figure 3.3. CO partial pressure profiles for *R. rubrum* in Experiment 2.

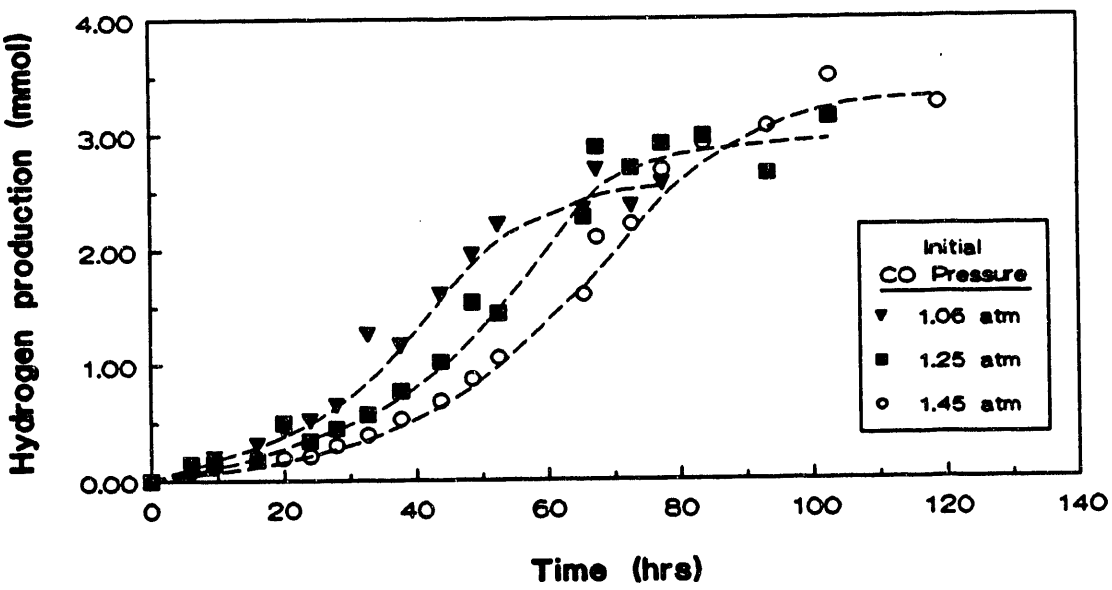

Figure 3.4. H_2 production for *R. rubrum* in Experiment 1.

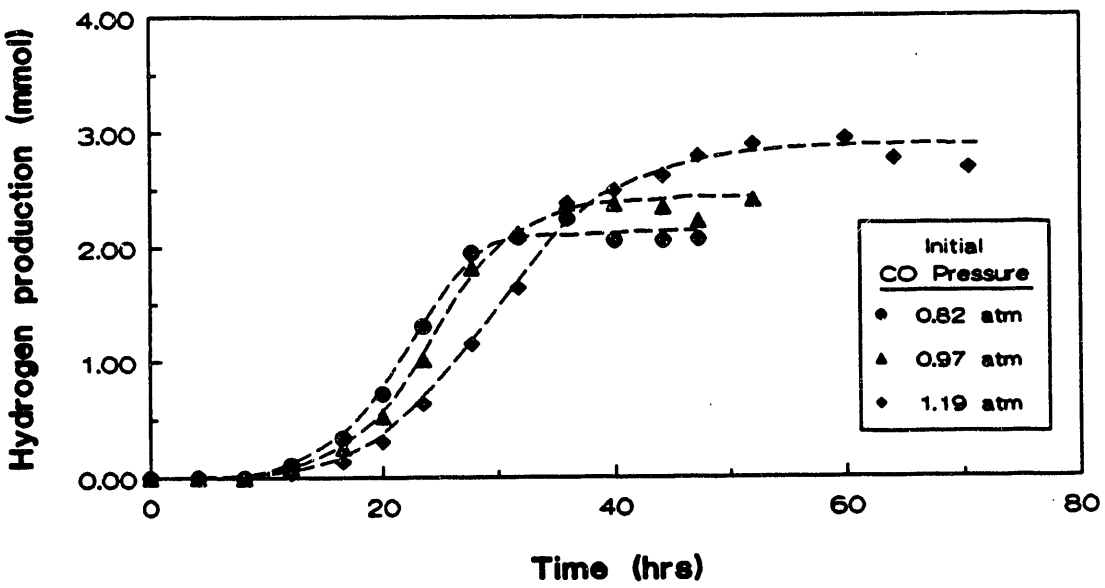

Figure 3.5. H_2 production for *R. rubrum* in Experiment 2.

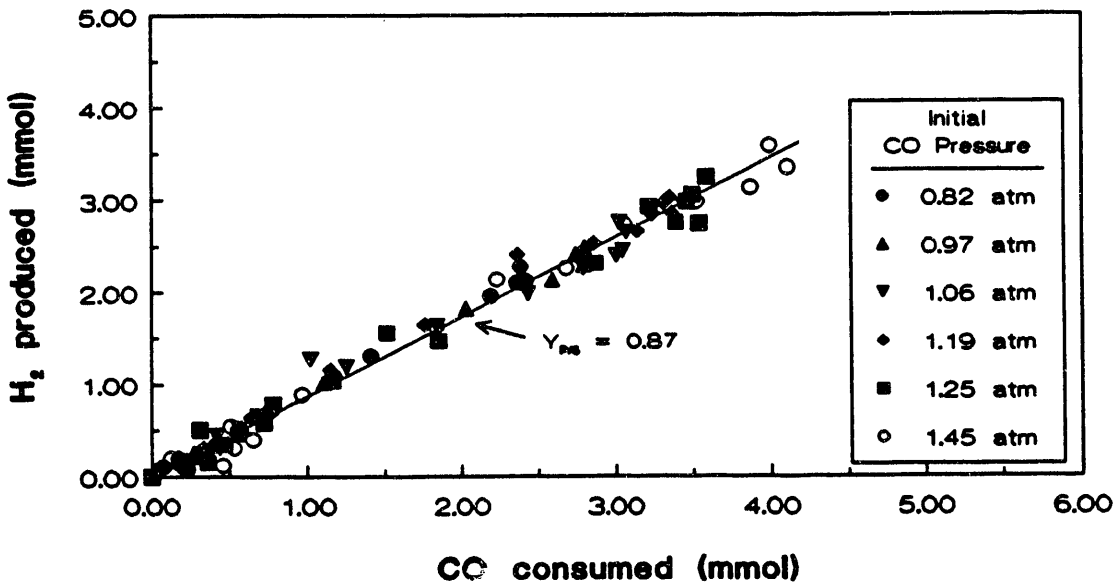

Figure 3.6. Estimation of the H_2 yield on CO for *R. rubrum* in Experiments 1 and 2.

(1.3). Two possible explanations for this low yield may be that *R. rubrum* may use some of the electrons for other than H_2 production or that some of the CO may have been used as a carbon source by the cells.

Figure 3.7 was generated in order to illustrate the determination of the mass transfer coefficient. In Figure 3.7, the estimation K_La is performed only with data from Experiment 1. The slope of the straight line is equal to K_La/H and if a value of 1120 l atm/mol is used for the Henry's law constant (26), K_La may be determined as 9.7 hr^{-1} for this experiment. For the second experiment a K_La of 14.4 was obtained in a similar fashion With the values of K_La, the partial pressure of CO in the liquid may be found as described in Step 3 above and the plot suggested in Step 4 may be generated (see Figure 3.8). In Figure 3.8, the initial lag phase before exponential growth has been eliminated for all cases. As noted, all of the data may be represented by a single quadratic curve. From the coefficients in the equation of the curve, the parameters in Equations (3.4) and (3.5) may be easily calculated. The final expression correlating the specific uptake rate of CO by *R. rubrum* is described in Equation (3.6).

$$q = \frac{0.055\ p_L^*}{0.45 + p_L^* + \left[p_L^*\right]^2/0.106}\ , \quad (p_L^* < 1.1\ \text{atm}) \qquad (3.6)$$

In examining Equation (3.6), it is seen that the maximum specific uptake rate of CO, q_m, is 0.055 mol/g,hr and the Monod constant, K_p, is 0.45 atm. In addition, the substrate inhibition constant, W, has a value of 0.106 atm, indicating that CO significantly inhibits CO uptake. In fact, the highest specific uptake rate found from Equation (3.6) is 0.011 atm, occurring at an equilibrium partial pressure of 0.218 atm.

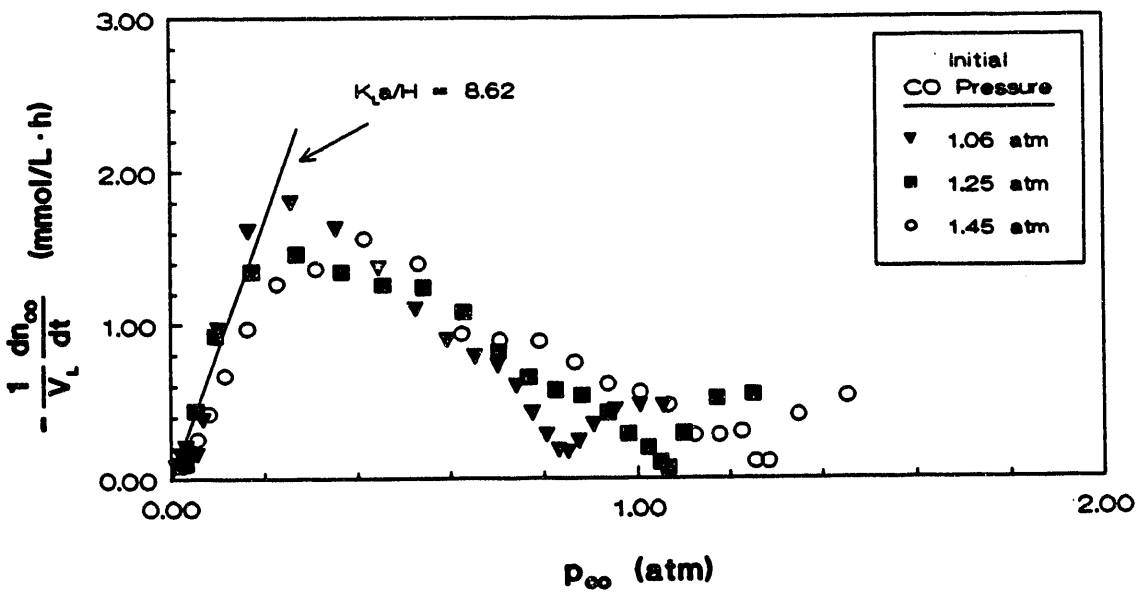

Figure 3.7. Determination of the mass transfer coefficient for *R. rubrum* in Experiment 1.

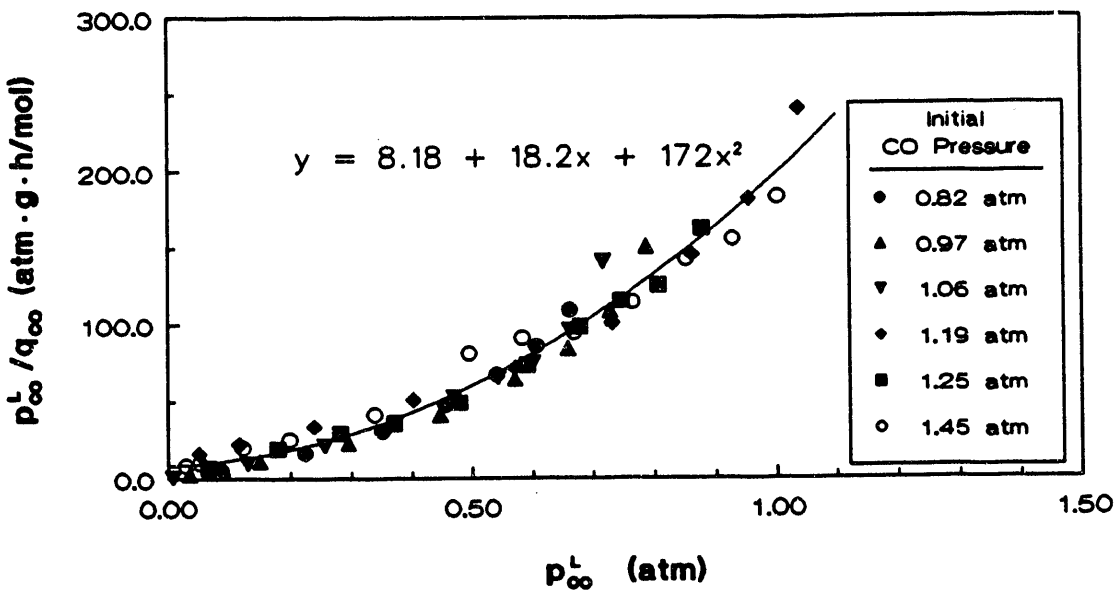

Figure 3.8. Determination of the kinetic parameters for CO uptake by *R. rubrum* according to the proposed model (Experiments 1 and 2).

In comparing the rate of H_2 production on CO by *R. rubrum* with H_2 production by other organisms, it is seen that *R. rubrum* has a specific H_2 production rate (equal to 87% of the CO uptake rate) of 0.004-00.009 mol/g, hr over an equilibrium partial pressure range of 0.1-1.0 atm. In a review article, Vignais *et al.* (27) reported maximal H_2 production rates by a variety of photosynthetic bacteria on various substrates. The highest reported H_2 production rate was 0.010 mol/g,hr for *Rhodopseudomonas capsulata*, strain B10, grown on lactate in nitrogen-limited culture. Bott *et al.* (28) reported a H_2 production rate of 2.4×10^{-3} - 3.6×10^{-3} mol/g, hr for *Methanosarcina barkeri* grown on 2.5-10% CO at pH 7 and 37°C in the presence of propyl iodide and 2-bromoethanesulfonate.

3.2 The Effect of Light Intensity on Growth for *R. rubrum*

Studies of bacterial growth are often conducted in batch fermentation vessels or chemostats with one limiting nutrient, usually carbon. Light is generally not considered a nutrient but may be the growth limiting factor in the photosynthetic growth of suspended cells. The role of light intensity and its influence on growth and product formation has mainly been studied with algae (29-31) and various mathematical models have been proposed (32) and tested. The most often used correlation is a Monod type equation using the mean light intensity as the limiting "nutrient."

All purple bacteria are potentially capable of growing anaerobically in the light with CO_2 as the carbon source and inorganic compounds as electron donors. However, the purple bacteria can also utilize acetate (or other carbon sources) under similar conditions for photohetrotrophic growth. The acetate is largely converted into a reserve material, poly-β-hydroxybutyric acid, in stepwise reactions which may be summarized as:

$$2nCH_3COOH + 2nH + 2nATP \rightarrow (C_4H_6O_2)_n + 2nH_2O + 2nADP + 2nP_i \quad (3.7)$$

The reduction power needed (H) may be supplied from the TCA cycle, with the anaerobic oxidation of acetate according to the equation:

$$CH_3COOH + 2H_2O \rightarrow 2CO_2 + 8H \quad (3.8)$$

The necessary ATP is furnished through the photochemical reaction:

$$ADP + P_i + Light \rightarrow ATP \quad (3.9)$$

The overall reaction obtained by combining Equations (3.7-3.9) yields:

$$9nCH_3COOH + Light \rightarrow 4(C_4H_6O_2)_n + 2nCO_2 + 6nH_2O \quad (3.10)$$

As is seen in Equation (3.10), most of the carbon present in acetate is converted to poly-β-hydroxybutyrate and very little is lost as CO_2. However, since poly-β-hydroxybutyrate itself is not cell material, further carbon will be lost as CO_2 in the sequential steps.

Since the generation of energy and thus growth is dependent upon light it should be possible to treat the light intensity as a "substrate" and utilize a Monod type expression to predict the specific growth rate (μ) with light intensity (29,32,33) This relationship is shown in Equation (3.11):

$$\mu = \frac{\mu_m I}{K_I + I} \quad (3.11)$$

However, the light intensity (I) is very different from a substrate since it varies throughout the bulk of the liquid. For dense cultures it is therefore necessary to use either an average specific growth rate (32) or, if the circulation of liquid throughout the bottle is high, an average light intensity (29,31). The resulting equations when using an average specific growth rate and an average light intensity are shown below in Equations (3.12) and (3.13).

$$\mu_{avg} = \frac{1}{L} \int_0^L \mu(I_z)\, dz \qquad (3.12)$$

$$I_{avg} = \frac{1}{L} \int_0^L I_z\, dz \qquad (3.13)$$

I_z may be described by the well-known Beer-Lambert law

$$I_z = I_o\, e^{-\epsilon z X} \qquad (3.14)$$

where I_o is the incoming light intensity, z and X are the light path distance and the cell concentration, respectively, and ϵ is the extinction coefficient.

If, on the other hand, the cell concentration is low and the agitation vigorous in a small vessel, it may be assumed that the effect of light intensity on the specific growth rate may be expressed in terms of incoming light intensity (see Equation (3.15)). This is true if the mixing time is faster than the growth rate. In other words, the cells will be in a region (volume) close to the incoming light, often enough not to be affected by the reduced light throughout the culture. In the case of dense cultures, this region becomes very small and the incoming light is quickly reduced, so that it is likely the cells will enter this smaller region often.

$$\mu = \frac{\mu_m I_o}{K_I + I_o} \qquad (3.15)$$

In Equation (3.15), μ may be estimated as 1/X)(dX/dt) during the initial part of a batch experiment when the cell concentration is low. Equation (3.15) may be rearranged to yield a linear form as:

$$\frac{1}{\mu} = \frac{1}{\mu_m}\left[\frac{1}{I_o}\right] + \frac{K_I}{\mu_m} \qquad (3.16)$$

Equation (3.16) may be used to estimate the constants μ_m and K_I using a straight line regression fit.

Two batch experiments were conducted with a set of five reactors per experiment. Using natural grey light reduction filters, various incoming light intensities were achieved. The cell concentration (X) was obtained as a function of time and these cell concentration profiles are shown in Figure 3.9 for one of the experiments. As is noted in Figure 3.9, growth increased with increasing light intensity. The initial specific growth rate for each reactor was estimated with increasing light intensity. The initial specific growth rate for each reactor was estimated as the slope of the line from a plot of ln(X) as a function of time. A typical growth curve is shown in Figure 3.10 and, as is seen in the insert in Figure 3.10, the slope (μ) of the curve decreases with time as the culture gets more dense and the incoming light is significantly reduced. The initial specific growth rates determined by the procedure demonstrated in Figure 3.10 for the various light intensities are shown in Table 3.2.

Using the values in Table 3.2 and the relationship presented in Equation (3.16), the values for the parameters μ_m and K_I were found to be 0.052 h^{-1} and 140 lux, respectively. This indicates a maximum specific growth rate of 0.052 h^{-1} for the conditions employed and a 50% reduction of the maximum growth rate at a light intensity of 140 lux. In Figure 3.11, the initial specific growth rate is plotted as a function of light intensity. The curve in Figure 3.11 is obtained from the empirical model

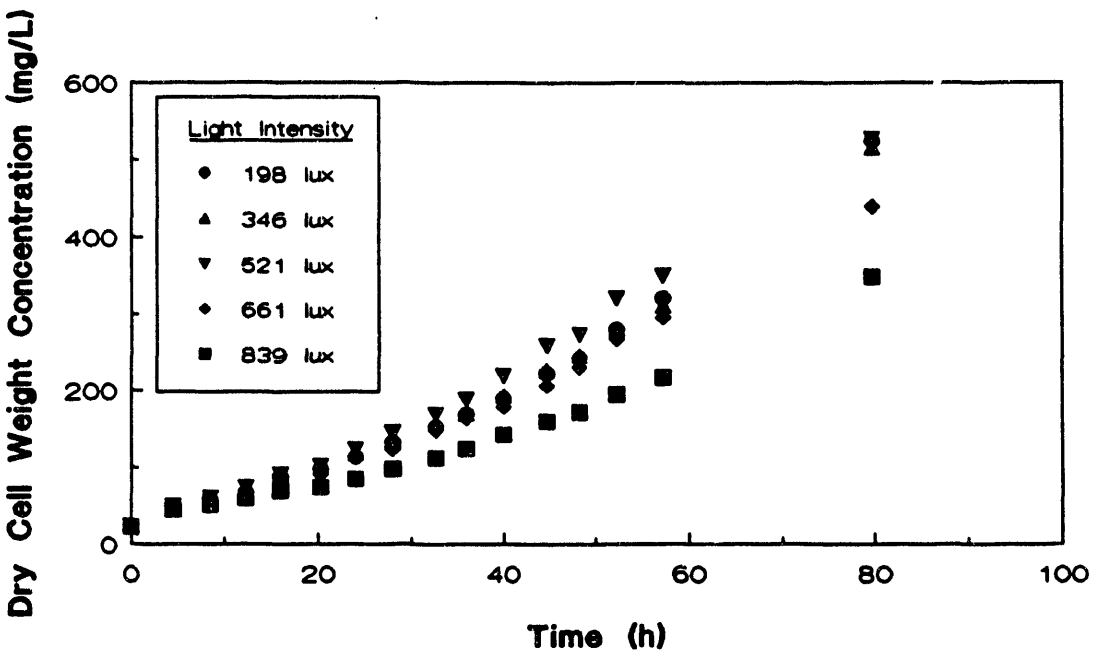

Figure 3.9. Cell concentration profiles at various light intensities for *R. rubrum*.

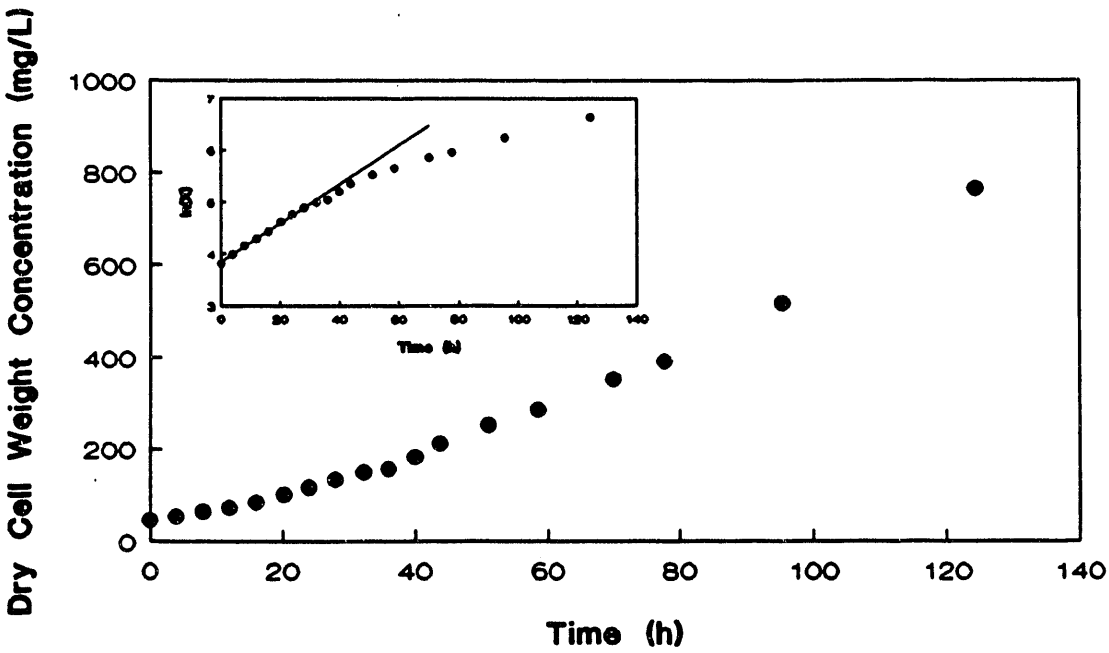

Figure 3.10. Cell concentration profile and determination of initial specific growth rate for *R. rubrum* in an experiment using a light intensity of 507 lux.

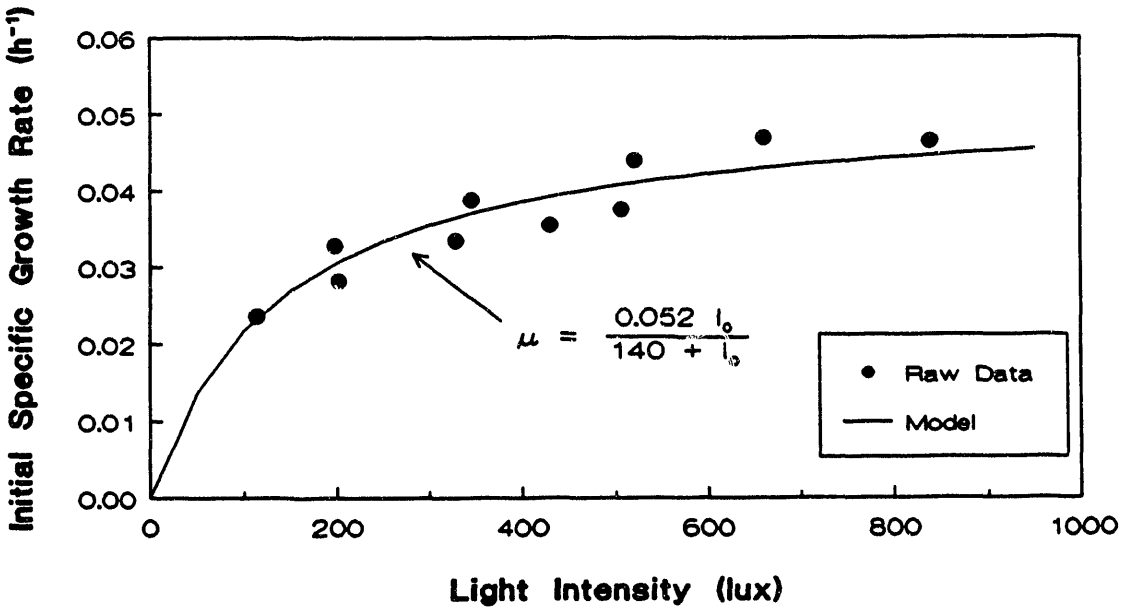

Figure 3.11. The effect of light intensity on the initial specific growth rate for *R. rubrum*.

$$\mu = \frac{0.052\ I_o}{140 + I_o} \qquad (3.17)$$

Table 3.2

The Effect of Light Intensity (I_o) on Initial Specific Growth Rate (μ_{init}) for *R. rubrum*

Experiment I		Experiment II	
I_o(lux)	$\mu_{init}(h^{-1})$	I_o(lux)	$\mu_{init}(h^{-1})$
198	0.0328	114	0.0236
346	0.0388	202	0.0282
521	0.0439	329	0.0334
661	0.0469	430	0.0355
839	0.0464	507	0.0375

As is noted, a good correlation is obtained between the raw data and the predicted values obtained from the correlation. The specific growth rate asymptotically approaches the maximum specific growth rate of 0.052 h^{-1} as predicted by the model and, at a light intensity of 2660 lux, the specific growth rate is 95% of the maximum. The effect of light intensity on growth and the chlorophyll content of *R. rubrum* was also studied by Holt and Marr (34). They found a similar shaped curve as presented in Figure 3.11 when plotting the specific growth rate as a function of light intensity. In continuous stirred tank reactor experiments using a malate-glutamate medium (the preferred medium for *R. rubrum*), specific growth rates of 0.13-0.14 h^{-1} for light intensities above 4300 lux were obtained. A very sharp decrease in

the specific growth rate below 1000 lux was also observed. Later, Cohen-Bazire and Sistrom (35) used the data from Holt and Marr together with additional data from experiments with *Rhodopseudomonas spheroides* to describe the specific growth rate as a function of light intensity. According to their preliminary results, the specific growth rate could be described as μ_m-B/I, where I is the light intensity and B is an empirical constant. Direct comparisons of the present results with data in the literature are difficult due to differences in medium, reactor shape, light intensity measurements and light source. Qualitatively, however, the effect of light intensity on the specific growth rate appears to follow a Monod type shaped curve for all of the systems studied. This clearly indicates the importance of light intensity in photosynthetic microbial systems and the resemblance between light intensity and a limiting substrate.

In addition to the light limiting culture experiments, experiments were also conducted with excess light in which acetate and ammonia concentrations were limited. Cell growth is plotted as a function of acetate and ammonia consumption in Figures 3.12 and 3.13, respectively. A straight line fit through the origin was used in both cases to find the observed cell yield on acetate and ammonia. The cell yields were calculated to 0.42 g/g and 13 g/g for acetate (as acetic acid) and ammonia (as NH_3), respectively. Based upon an empirical chemical formula for bacterial cells ($CH_{1.833}N_{0.225}O_{0.385}$) (36), approximately 55% of the carbon in acetate was incorporated into cell mass, with the balance going to CO_2.

3.3 The Effect of Temperature on the Kinetics of *R. rubrum*

The models of Equations (3.6) and (3.17) were obtained at the published optimum temperature of 30°C. However, from observing the performance of other

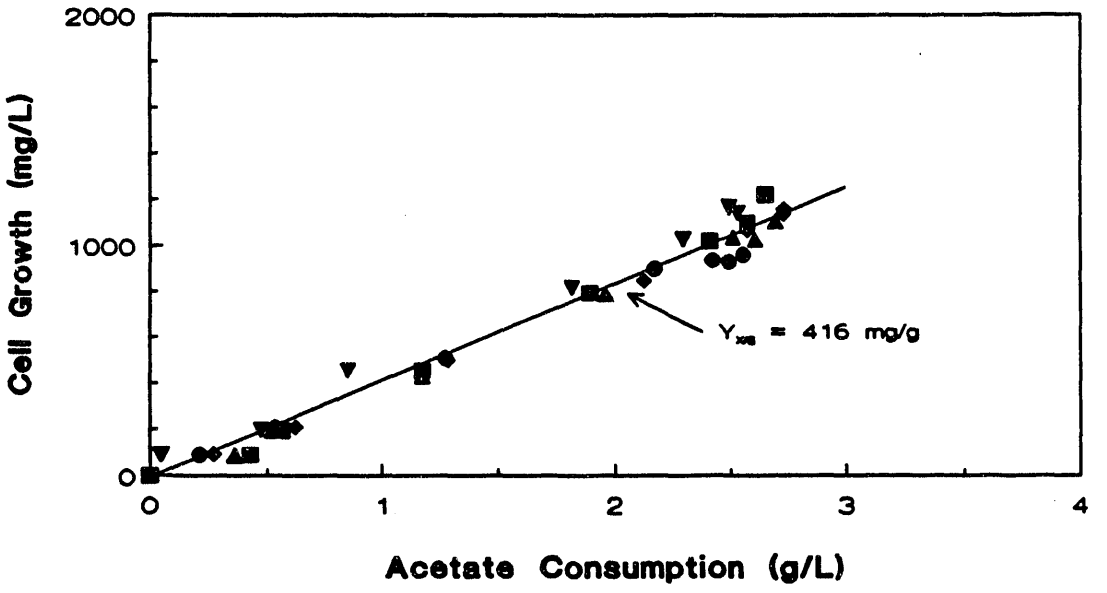

Figure 3.12. Determination of the cell yield on acetate for *R. rubrum*.

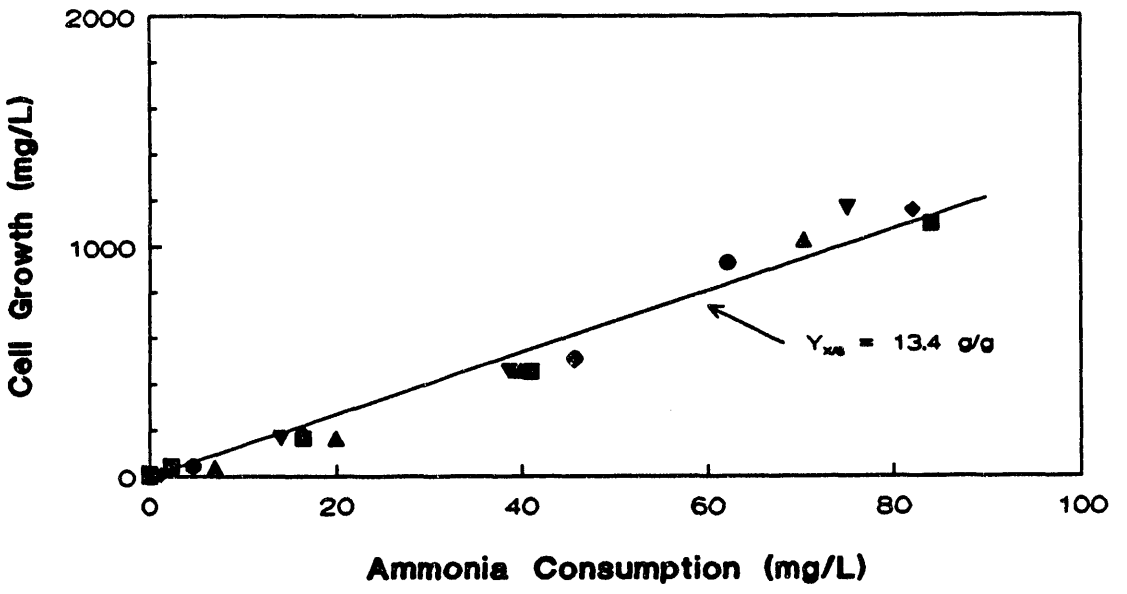

Figure 3.13. Determination of the cell yield on ammonia for *R. rubrum.*

microorganisms as a function of temperature it was often found that the reported optimum was, in fact, not really an "optimum" temperature, but instead a "preferred" temperature of the two or three temperatures tested. Thus, the effects of temperature on growth and uptake by *R. rubrum* need to be studied to establish true temperature optima in terms of maximizing the specific growth and uptake rates. Furthermore, since biological water gas shift may not be carried out under strictly isothermal conditions in industrial reactors, the effect of temperature on the performance of the bacterium needs to be well understood.

The purpose of this study is to present results on the effect of operating temperature on the performance of *R. rubrum*. The operating temperature was varied between 25 and 37°C in an effort to quantify the effects of temperature on the specific growth rate, the yield of H_2 from CO and specific uptake kinetics.

Five temperatures were considered in the experimental study: 25, 30, 32, 34 and 37°C. As was mentioned previously, the reported "optimum" temperature was 30°C. Thus, temperatures both above and below the optimum were considered. The lowest temperature chosen was 25°C since it is well known that reaction rate generally increases with temperature, so that the specific rates of both growth and uptake would be expected to be quite low at temperatures below 25°C. The maximum temperature studied was 37°C since no growth was obtained at this temperature. Small temperature increments between 30 and 37°C were used since it was expected that these small increases in temperature might significantly affect bacterial growth and CO uptake.

The effects of temperature on cell concentration in the exponential growth phase is shown in Figure 3.14, where the natural logarithm of the cell

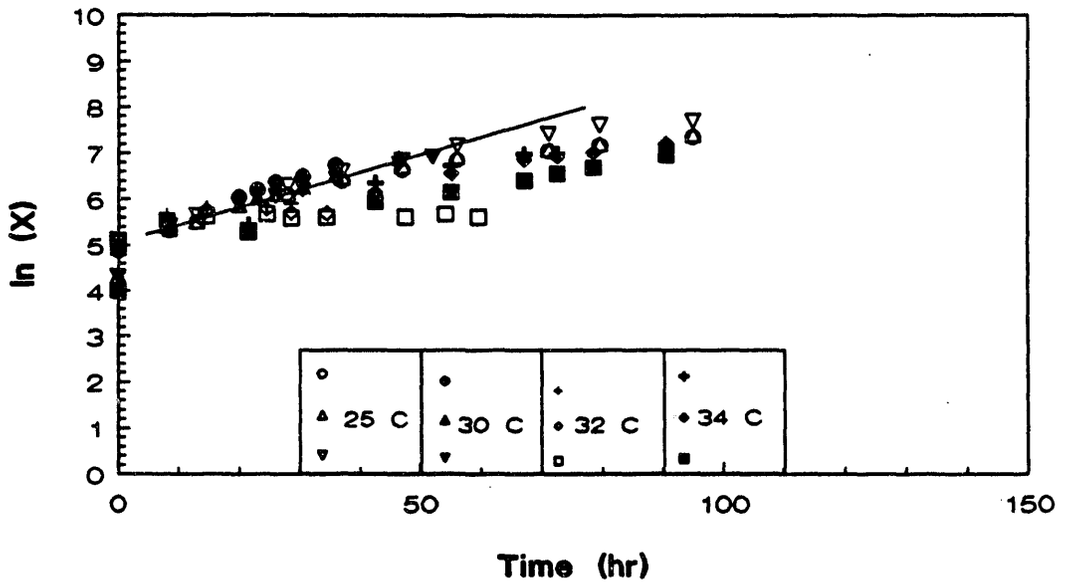

Figure 3.14. Growth of *R. rubrum* in the experimental growth phase as a function of temperature.

concentration is plotted as a function of time for four temperatures. Again, no growth was observed at 37°C. The experimental growth region was chosen for analysis in order to eliminate differences in inoculum and culture acclimation effects often present in the lag phase. In the exponential phase, the plot of ln X as a function of time should yield a straight line. As is noted in Figure 3.14, three experiments (corresponding to three initial partial pressures) were run at each temperature. In analyzing the data, it is seen that the highest cell concentrations (ln X) occurred at the lower temperatures of 25 and 30°C. Slightly depressed growth occurred at 32 and 34°C. If a single straight line is drawn through the truly exponential region of the data, the slope of the line is found to be 0.035 h^{-1}, which is equal to the specific growth rate, μ. Thus, any temperature between 25 and 34°C is suitable for the growth of *R. rubrum*.

Figure 3.15 shows the calculation of the yield of H_2 from CO, $Y_{P/S}$, for the four temperatures. Previous results have shown a product yield of 0.87 mol/mol at 30°C, and the theoretical yield is 1.0 mol/mol from Equation (3.6). The slope of the line in Figure 3.15 is 0.96, which is 96% of theoretical. Also, there is seen to be no effect of temperature on the product yield. No explanation is offered for the increase in the yield in the temperature study compared with previous results at 30°C.

A plot of P_{CO}^{G}/q as a function of P_{CO}^{G} is shown in Figure 3.16 for the four temperatures. As is noted, a single curve is essentially obtained for temperatures of 30, 32 and 34°C, indicating that the specific uptake rate is the same at these temperatures. (An exception to this observation is one set of data at 34°C which gives lower uptake rates and thus higher values of P_{CO}^{G}/q. Also, the rather steep curvature for one set of data at 30°C is due

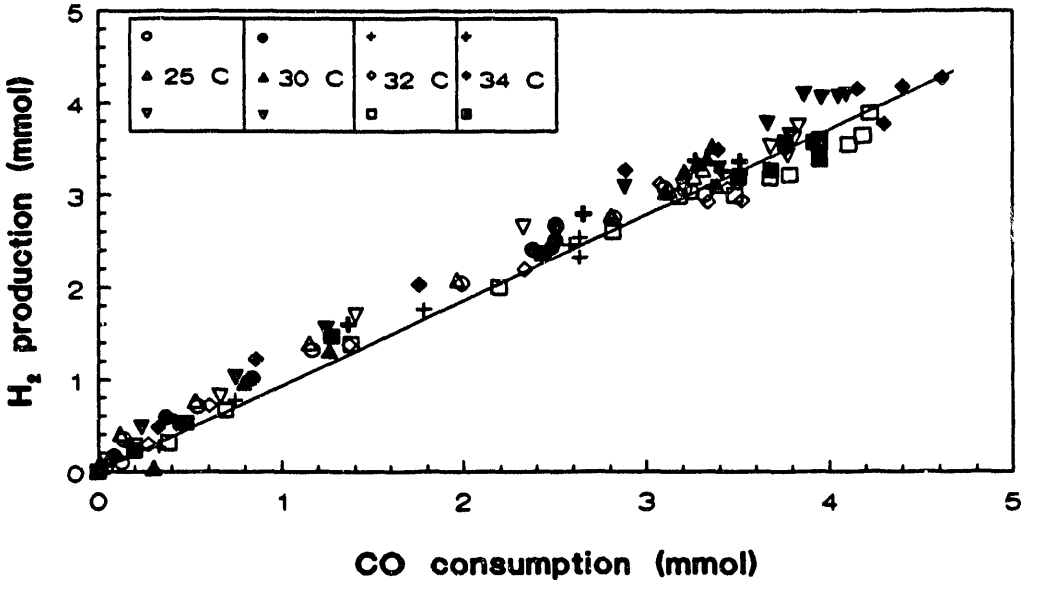

Figure 3.15. Calculation of the yield of H_2 from CO by *R. rubrum* as a function of temperature.

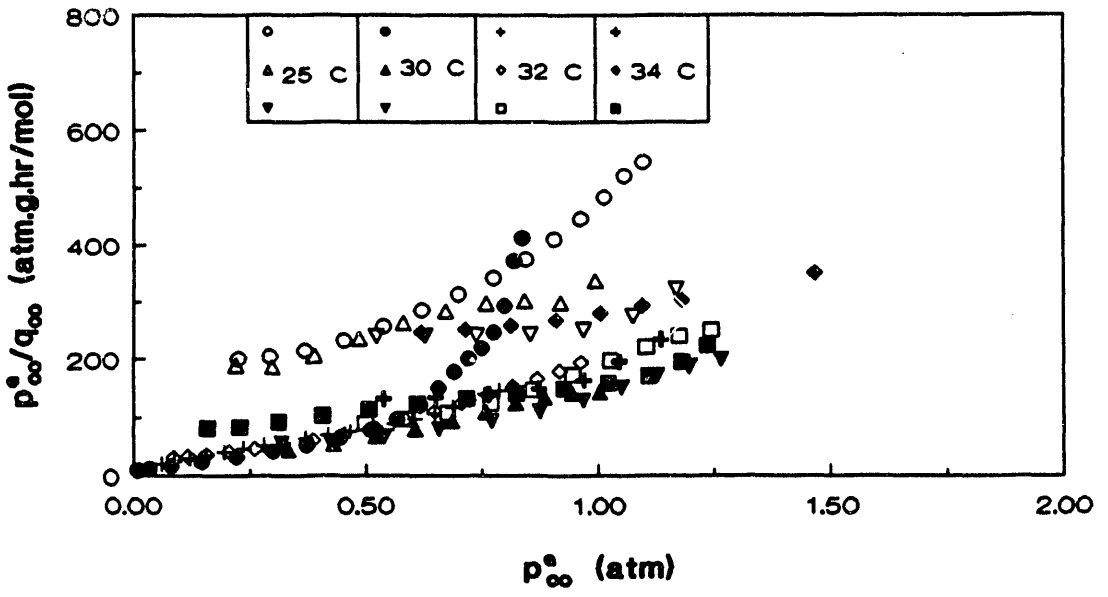

Figure 3.16. Comparison of specific uptake kinetics for *R. rubrum* as a function of temperature.

to the lag phase). At 25°C, it is seen that the specific uptake rate is lower for all three data sets, indicating that 25°C would be an inappropriate temperature for catalyzing the reaction of Equation (3.6).

Thus, the growth of *R. rubrum* may be satisfactorily carried out at 25 and 30°C, while uptake and thus the conversion of CO best occurs at temperatures of either 30, 32 or 34°C. The reported optimum of 30°C is well suited for both growth and CO uptake. More importantly, small upward variations in temperature in industrial processes will not negatively affect CO uptake or H_2 production.

3.4 The Kinetics of *R. rubrum* in the Continuous Stirred Tank Reactor

The purpose of this study was to determine the CO conversion kinetics by *R. rubrum* in a continuous stirred tank reactor and to illustrate the potential for using *R. rubrum* as a model system for the mass transfer determinations. The experiments were conducted in a fashion which allowed for separation of mass transfer and kinetic aspects of the fermentation.

An overall non-steady state CO balance over the CSTR may be written as:

$$\left[\frac{P^I_{Ar} G^I}{R\,T}\right]\left[\left[\frac{P^I_{CO}}{P^I_{Ar}}\right] - \left[\frac{P^G_{CO}}{P^G_{Ar}}\right]\right] - \left[\frac{V_G}{R\,T}\right]\frac{dP^G_{CO}}{dt} = r_{CO} V_L \qquad (3.18)$$

where r_{CO} is the volumetric CO mass transfer/uptake rate as defined in Equation (3.19).

$$r_{CO} = K_L a \left[C^*_L - C_L\right] = \left[\frac{K_L a}{H}\right]\left[P^G_{CO} - P^*_{CO}\right] = Xq\left\{P^*_{CO}\right\} \qquad (3.19)$$

The function $q\left\{P^*_{CO}\right\}$ in the above equation describes the microbial kinetics

and may be as simple as a Monod-type expression or may include additional terms.

Based on gas analysis, r_{CO} may be calculated from Equation (3.18) for the entire fermentation. As the cell concentration increases with time, the system moves fro a kinetic limited condition to a mass transfer limited state. At this point the CO conversion (and r_{CO}) becomes constant even though the cell concentration still increases. The mass transfer coefficient can now be calculated using Equation (3.19) with the assumption that $P^*_{CO} << P^G_{CO}$. It is important to realize that the growth of *R. rubrum* is not limited by the CO supply but by liquid constituents, liquid flow rate and illumination. The same equation may then be used to estimate the dissolved CO $\left(P^*_{CO}\right)$ for the earlier part of the fermentation. Finally, with the calculated values of r_{CO}, P^*_{CO} and the measured values of X, Equation (3.19) may again be used to evaluate the kinetic function, $q\left\{P^*_{CO}\right\}$.

Experiments were conducted using five different agitation rates (300-700 rpm in 100 rpm increments). Gas composition and cell concentrations were measured. In Figure 3.17, representative CO conversion and cell concentration profiles for three of the five experiments are displayed. As is noted in the figure, an increase in the agitation rate resulted in a higher value for the maximum conversion at a given agitation rate. A maximum CO conversion of 38% was obtained using an agitation rate of 300 rpm compared to a 58% CO conversion at 700 rpm. The maximum CO conversion, indicated by the plateau obtained for the CO conversion profiles (see Figure 3.17), corresponds to CO mass transfer limiting conditions in the fermenter. It is clear that mass transfer limiting conditions are in effect during this time since the CO

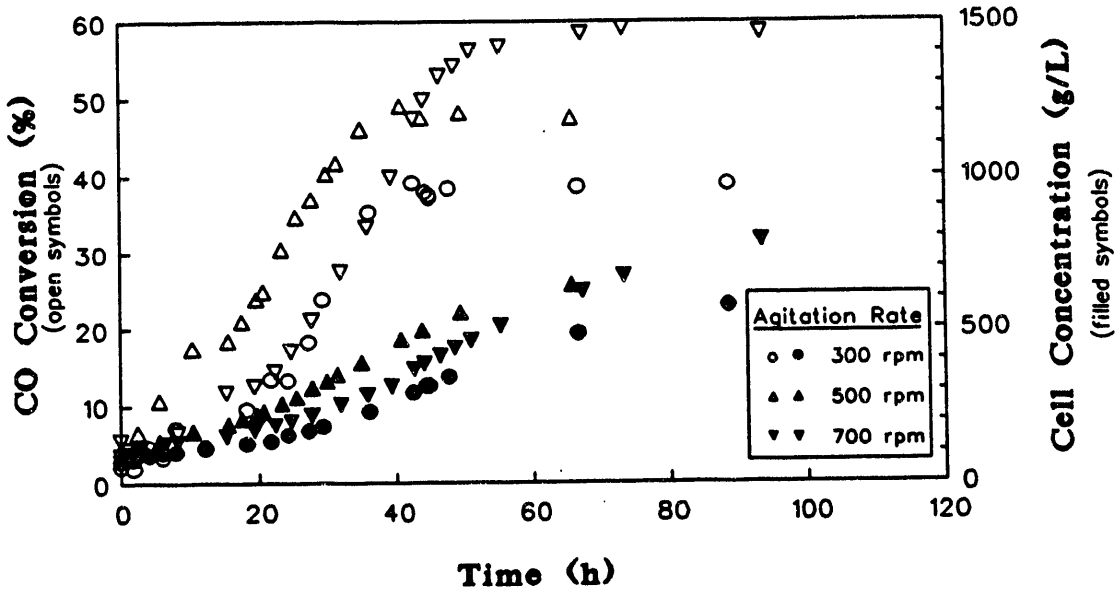

Figure 3.17. Cell concentration and CO conversion profiles in the CSTR for agitation rates of 300, 500, and 700 rpm *(R. rubrum)*.

conversion leveled off even though cell concentration continued to increase. Thus, the cell concentration in the fermenter was not limited by CO transport but by the factors described above. By the same token, the maximum CO conversion was not limited by cell concentration but by agitation rate, gas flow rate and gas inlet composition.

Based on the gas phase analysis, the volumetric CO transfer rate (r_{CO}) was calculated according to Equation (3.18) for the mass-transfer limited region of the fermentation (time > 45-60 h). The overall mass transfer coefficients were then calculated using Equation (3.19) and the assumption that $P^*_{CO} << P^G_{CO}$. The estimation K_La values ranged from 15 to 35 h^{-1} for the agitation rate range of 300-700 rpm (see Table 3.3). For agitation rates between 400-600 rpm, only small changes in the K_La values were observed. The most likely explanation for this result is that the position of the impellers relative to the liquid level and the effect of vortex mixing is of great importance. Visual inspection showed a clear change in flow patterns between 300 and 400 rpm, and 600 and 700 rpm.

By using the calculated values of r_{CO} (from Equation (3.18) and the estimated values of K_La (see Table 3.3), the dissolved CO concentration $\left[P^*_{CO}\right]$ was calculated for the initial (and assumingly kinetic limited) part of the fermentation using Equation (3.19). A representative result is shown in Figure 3.18 for an agitation rate of 500 rpm. As is noted, P^*_{CO} was approxmately zero after 45 hours, corresponding to mass transfer limited operation. In addition to calculating P^*_{CO}, the values for the specific CO uptake rate (q) equal to r_{CO}/X, were also calculated (see Figure 3.19). Starting of P^*_{CO}, the data indicated that the specific CO uptake rate increased

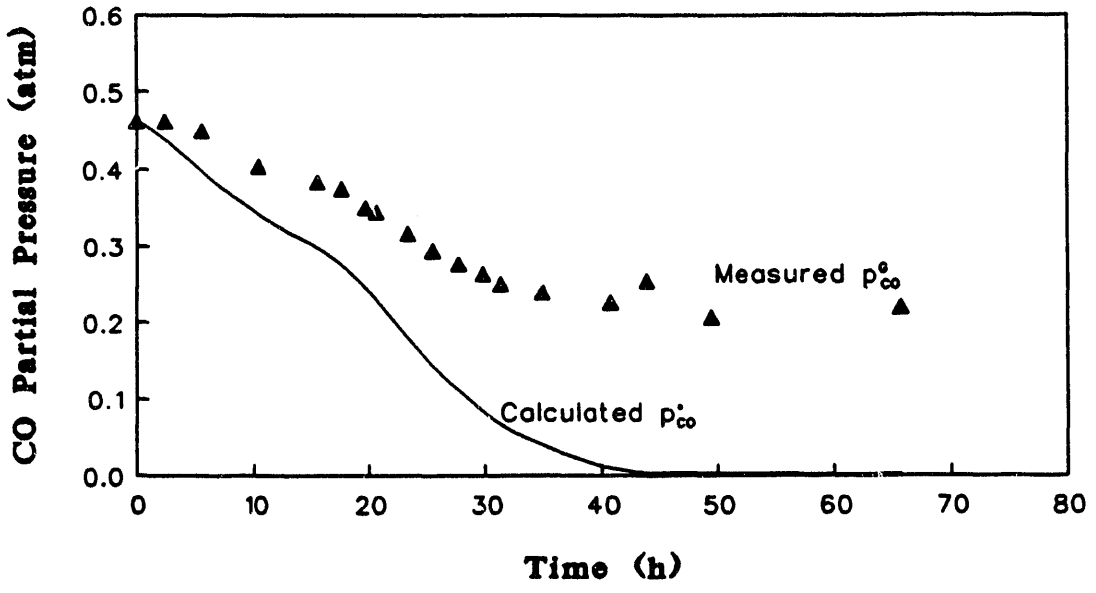

Figure 3.18. Measured CO partial pressure and calculated dissolved CO tension in the CSTR for an agitation rate of 500 rpm *(R. rubrum)*.

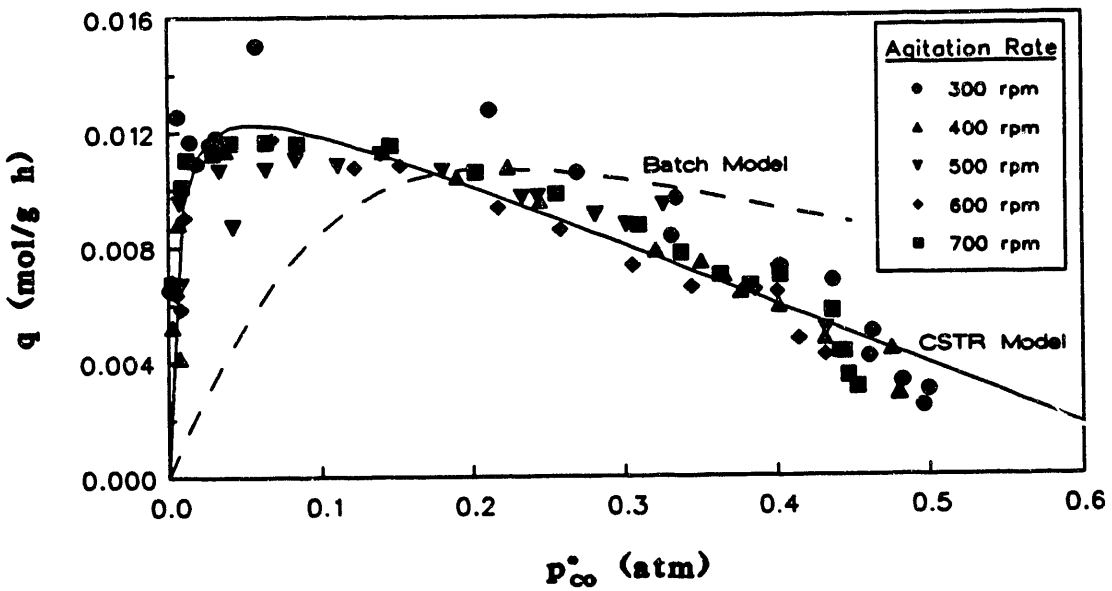

Figure 3.19. Measured specific uptake rate as a function of calculated dissolved CO tension for agitation rates of 300–500 rpm *(R. rubrum)*.

sharply with increasing values of P^*_{CO}. Above a dissolved CP pressure of 0.05 atm, the specific uptake rate decreased almost linearly with increasing CO partial pressure. It is evident from the result that CO has an inhibitory effect on the CO uptake (see Figure 3.19). Thus, an attempt was made to fit the data to two inhibition models based on the Monod equation, one commonly used for substrate inhibition, another mostly used to account for product inhibition.

Table 3.3

Mass Transfer Coefficients Calculated at Final Conversion Values for Various Agitation Rates (*R. rubrum*)

Agitation Rate (rpm)	P^*_{CO} (atm)	r_{CO} (mol/h L)	K_La (h^{-1})
300	0.2804	$3.731 \cdot 10^{-3}$	14.9
400	0.2307	$4.431 \cdot 10^{-3}$	21.5
500	0.2134	$4.337 \cdot 10^{-3}$	22.8
600	0.2142	$4.549 \cdot 10^{-3}$	23.8
700	0.1679	$5.322 \cdot 10^{-3}$	35.5

$$q = \frac{q_m \cdot P^*_{CO}}{K_p + P^*_{CO} + \left[P^*_{CO}\right]^2/W} \qquad (3.20)$$

$$q = \frac{q_m \cdot P^*_{CO}}{K_p + P^*_{CO}} \left[1 - \frac{P^*_{CO}}{P_m}\right] \qquad (3.21)$$

Equation (3.20) corresponds to Andrews modification of the Monod relationship to include substrate inhibition (24) and Equation (3.21) is the Monod expression, modified with a linear inhibition term. Equation (3.20) has recently been used to describe CO uptake rate by *R. rubrum* in batch culture.

Non-linear regression analysis was used to obtain the parameters in Equations (3.20) and (3.21). The result of this analysis indicated that Equation (3.20) was unsuitable for the data since the regression predicted negative values for at least one parameter. This was considered inconsistent with the development of Equation (3.20). The solid curve in Figure 3.19 is the best fit determined according to Equation (3.21) and corresponds to the expression:

$$q = \frac{0.0146 \cdot P^*_{CO}}{0.0053 + P^*_{CO}} \left[1 - \frac{P^*_{CO}}{0.68}\right] \qquad (3.22)$$

This equation is very sensitive to the independent variable P^*_{CO}. For low values of P^*_{CO}, the part of the equation corresponding to the Monod model is dominating, while for higher values of P^*_{CO}, the linear inhibition term is more prevalent. It may be predicted from the equation that CO uptake completely inhibited by CO partial pressures of 0.68 atm and above.

The dashed curve in the same figure was generated based on previous results obtained in batch culture using similar experimental conditions. As is noted in Figure 3.19, the correlation previously found for batch data does not fit the data obtained in the CSTR experiments. The CO uptake rate in batch culture was less inhibited by dissolved CO and q approached zero as P^*_{CO} approached infinity. However, both models predict a maximum specific CO

uptake rate of approximately 0.011-0.012 mol/g,h. The difference in batch versus continuous data may be explained by CO acclimation. Batch experiments were typically started with CO partial pressures up to 1.6 atm. A long lag phase was always present at these pressures, but the cultures grew eventually. All experiments conducted in the CSTR were started at a maximum CO partial pressure of 0.5 atm. If higher initial CO partial pressures had been used in the CSTR studies, perhaps the results in the CSTR and in batch culture would have been similar.

The hydrogen yield was constant throughout the CSTR experiments at 0.88 mol/mol (see Figure 3.20). This value is 88% of the theoretical value obtained from the stoichiometry of Equation (1.3). In batch culture, the yield was estimated to 0.87 mol/mol.

3.5 Rate of H_2 Production by *R. palustris*

R. palustris, grown on a basal medium supplemented with glutamic and acetic acids, has shown promising results in releasing H_2 during growth. This section will concentrate on determining the rate of the production in the experiment.

The rate of production of many growth-related products in microbial systems may be described by the equation:

$$\frac{d(PV_L)}{dt} = \nu \cdot XV_L \qquad (3.23)$$

where ν is the specific production rate, X is the cell concentration V_L is the liquid volume, P is the product concentration and t is time. The specific production take, ν, may be a function of substrate and product concentrations, but for simplicity it will be assumed to be constant. If the derivative, $d(PV_L)/dt$, the cell concentration, X, and the liquid volume V_L, are known a

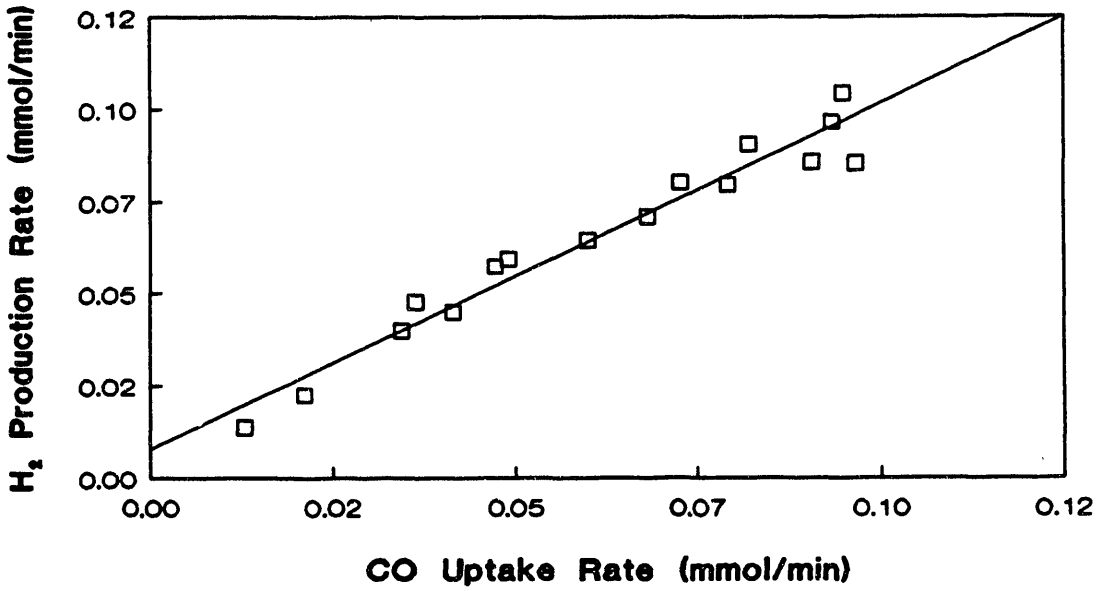

Figure 3.20. Determination of H_2 yield for *R. rubrum* in the CSTR.

value of ν may be found in Equation (3.23). For the case of hydrogen production from acetate by *R. palustris*, Equation (3.23) may be rewritten as:

$$\frac{dH_2}{dt} = \nu \cdot X \cdot V_L \qquad (3.24)$$

Batch cell concentration, H_2 production and liquid volume profiles are plotted for *R. palustris* in Figure 3.21. Also shown in the figure are smoothed curves of this data indicating experimental trends. Utilizing these smooth curves, the rates of hydrogen consumption dH_2/dt, were calculated. Figure 3.22 was constructed by plotting dH/dt as a function of XV_L. As is seen in the figure, a straight line may be used to predict the data for the initial part of the fermentation. The slope of the line, 0.002 mol/g,hr, is equal to the specific H_2 production rate, ν, by the cells. This value is considerably lower than the values of 0.004-0.009 mol/g,hr obtained for *R. rubrum* carrying out the water gas shift reaction. This result indicates that the water gas shift reaction using *R. rubrum* is the preferred choice over H_2 production from acetic acid in the presence of glutamic acid using *R. palustris*.

4.0 MASS TRANSFER AND KINETIC CONCEPTS WITH CHLOROBIUM THIOSULFATOPHILLUM

The anaerobic, photosynthetic bacterium *Chlorobium thiosulfatophilum* has been chosen from among several bacteria for its ability to convert H_2S to elemental sulfur. The bacterium utilizes CO_2 as its carbon source and operates at the mesophilic temperature of 37°C. The bacterium requires tungsten light for growth and compounds such as H_2S, elemental sulfur or H_2 as a source of reducing power. Of these latter three compounds, H_2S as sulfide is the preferred source of reducing power, with H_2 and elemental sulfur utilized only when sulfide has been depleted from the medium. The organism is

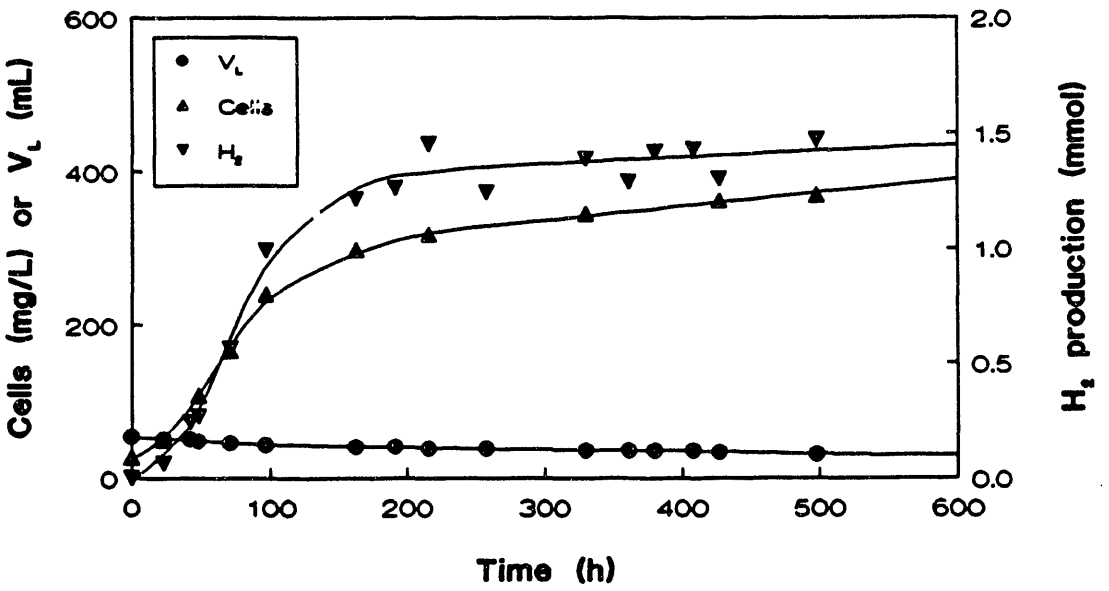

Figure 3.21. Cell concentration, H_2 production, and liquid volume profiles for *R. palustris* grown on glutamic and acetic acids.

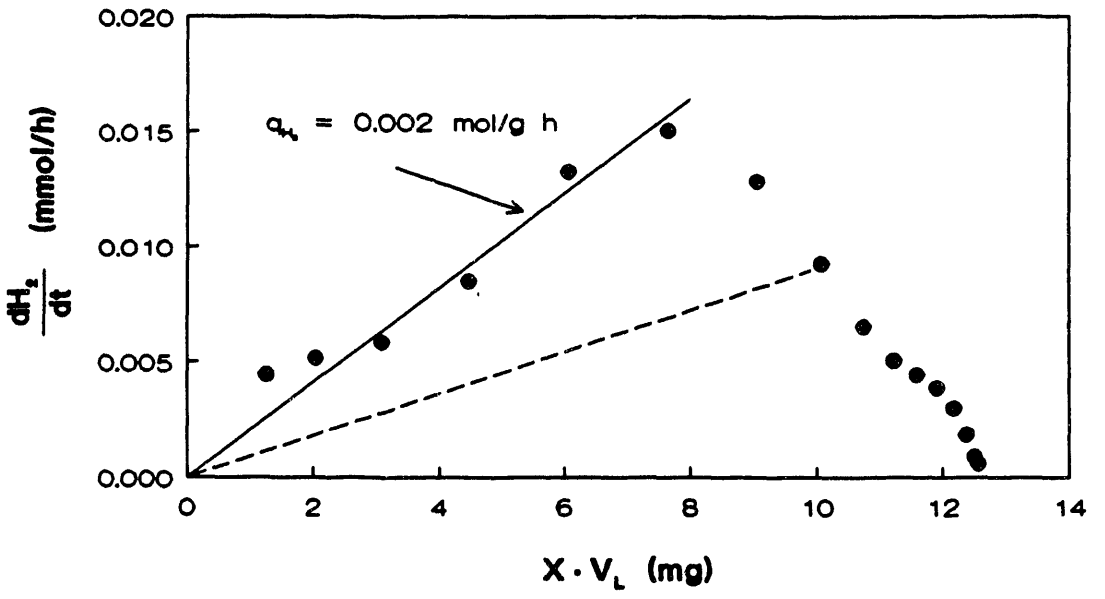

Figure 3.22. Determination of the average initial specific H_2 uptake rate for *R. palustris* grown on glutamic and acetic acids.

also capable of indirectly utilizing COS, since COS reacts with water to form CO_2 and H_2S by the equation (37):

$$COS + H_2O \rightarrow CO_2 + H_2S \qquad (1.4)$$

Thus, the H_2S formed by Equation (1.4) is utilized by *C. thiosulfatophilum* following the reaction of COS and water.

4.1 Growth of *C. thiosulfatophilum* in the Presence of H_2S

As was mentioned previously, *C. thiosulfatophilum* utilizes CO_2 as a carbon source, but also requires tungsten light and a source of reducing power such as H_2S, H_2 or elemental sulfur for growth. In the presence of H_2S, the sulfide is converted to elemental sulfur during growth.

To illustrate this interdependence of light, carbon source and reducing power a plot of the natural log of the ratio of the cell concentration compared to the initial cell concentration as a function of time is shown in Figure 4.1 for various initial H_2S levels. This plot should yield straight lines for each initial H_2S level, the slopes of these lines corresponding to the specific growth rate, μ, for each H_2S concentration. However, as is noted in Figure 4.1, essentially a single straight line is obtained for all of the H_2S levels. This result indicates that something other than H_2S is limiting the reaction. In this case, it is obvious that H_2S and CO_2 are present in excess and that the light intensity is limiting cell growth. It is thus expected that a Monod relationship for specific growth rate as a function of light intensity will be obtained.

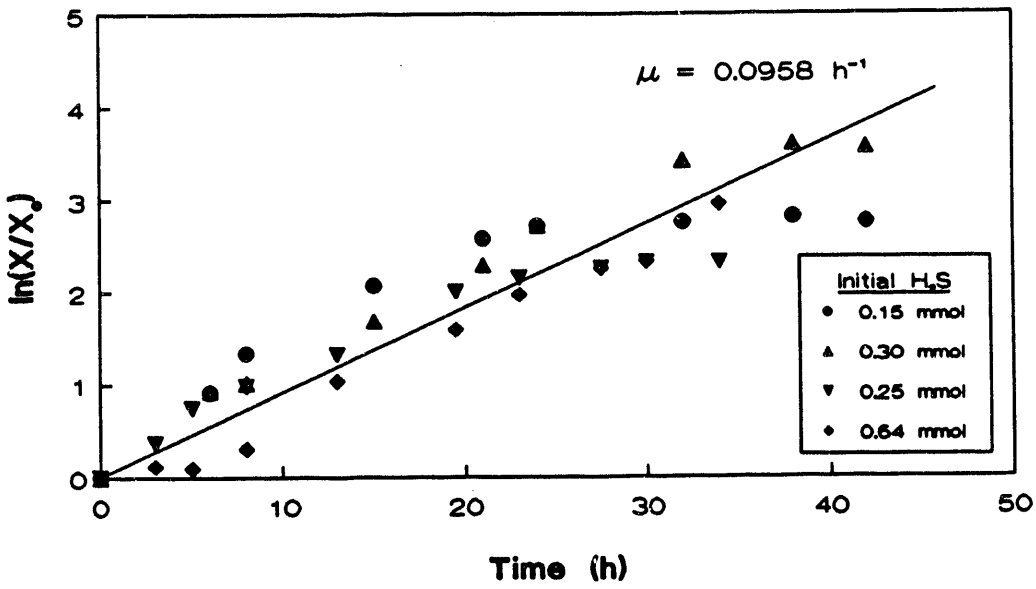

Figure 4.1. Determination of the specific growth rate of *C. thiosulfatophilum* at various initial H_2S levels.

The cell production by *C. thiosulfatophilum* as a function of the total sulfide concentration (H_2S (g), H_2S (l) and related species) is plotted in Figure 4.2 in order to determine the yield of cells from sulfide. As is noted, a single straight line is obtained for all of the initial H_2S levels, at least until H_2S is depleted from the system. When all of the H_2S is depleted from the medium, the culture continues to grow, utilizing elemental sulfur as the source of reducing power. This onset of elemental sulfur utilization is represented in Figure 4.2 by the vertical cell production data for each initial H_2S level.

As is noted in Figure 4.2, a cell yield on sulfide of 9.2 mg cells/mmol sulfide is obtained. This yield is greater than typical yields of cells from glucose by the yeast *Saccharomyces cerevisiae*, where a yield of 5.4-9.0 mgcells/mmol glucose is obtained.

A determination of Monod kinetics for H_2S uptake by *C. thiosulfatophilum* was not possible due to difficulties in following the various sulfur species and the problem associated with sulfur disappearance into the rubber septa sealing the batch reactors.

4.2 Loss of H_2S into Rubber Septa

Previous studies with H_2S uptake by various species of chlorobia have generated data which are difficult to quantify and model since H_2S is known to diffuse through the rubber septa sealing the batch reactors. Although H_2S disappearance into butyl rubber is relatively small in comparison to H_2S uptake by the bacteria, it would be helpful if the average amount of H_2S leaving the batch system through the stopper could be quantified.

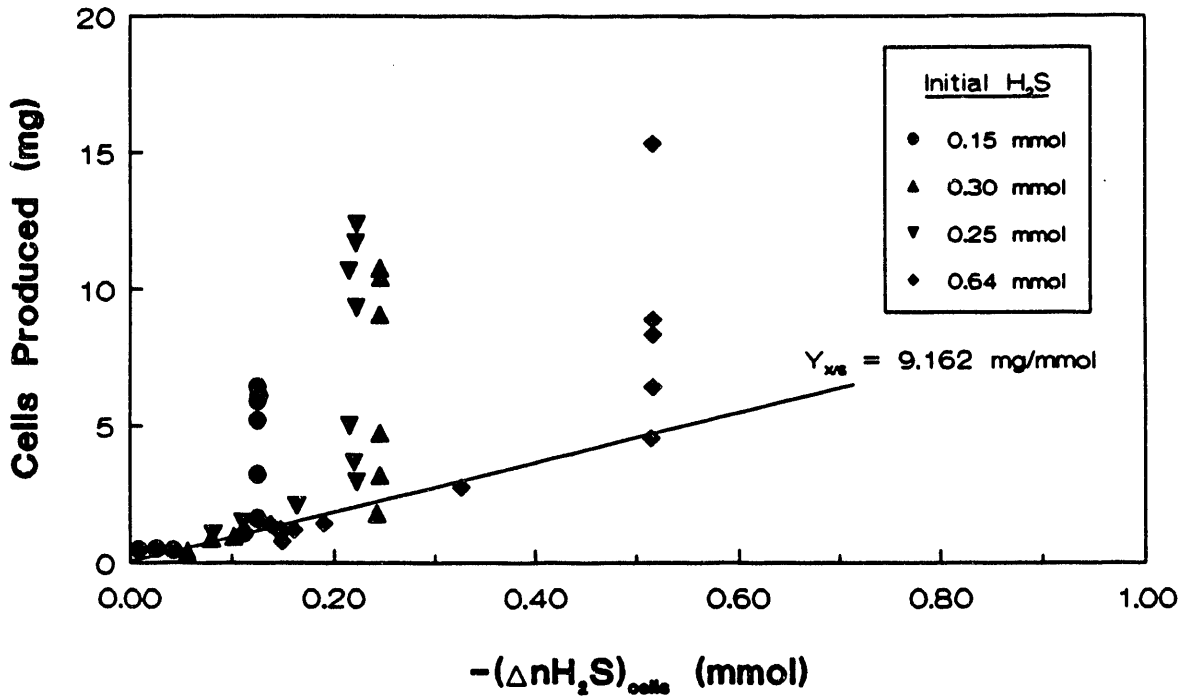

Figure 4.2. Cell Production by *C. thiosulfatophilum* as a Function of Sulfide Consumption.

If a first order rate of disappearance of H_2S (both gas and liquid species) is assumed, the following equation may be written:

$$- \frac{d(\text{sum } H_2S)}{dt} = k \; P^G_{H_2S} \qquad (4.1)$$

In Equation (4.1), $- \frac{d(\text{sum } H_2S)}{dt}$ represents the rate of disappearance of all sulfur species into the butyl rubber stoppers, $P^G_{H_2S}$ represents the gas phase partial pressure of H_2S and k represents the first order rate constant.

Equation (4.1) may be integrated to yield:

$$- \Delta \text{ (sum } \Delta H_2S) = k \int_o^t P^G_{H_2S} \, dt \qquad (4.2)$$

Thus a plot of $- \Delta$ (sum ΔH_2S) as a function of $\int_o^t P^G_{H_2S}$ should yield a straight line with a slope k if the disappearance can indeed be represented by a first order relationship.

Figure 4.3 shows such a plot for two initial H_2S levels in water (no culture), housed in serum stoppered batch reactors. As is noted, a reasonable straight line can be fitted through the data. The slope of this line, k, is 0.0470 mmol/atm•h. This relationship can now be used to correct experimental data for H_2S disappearance through the butyl rubber stoppers.

4.3 Indirect COS Uptake by *C. Thiosulfatophilum*

As was mentioned previously, COS undergoes a chemical reaction with water to produce H_2S and CO_2 by the equation:

$$COS + H_2O \rightarrow CO_2 + H_2S \qquad (1.4)$$

Thompson *et al.* (37) studied the reaction and showed that the kinetics of the reaction could be described by a first order irreversible rate expression over a temperature range of 15-40°C. They showed that the rate constant varied with temperature by the equation:

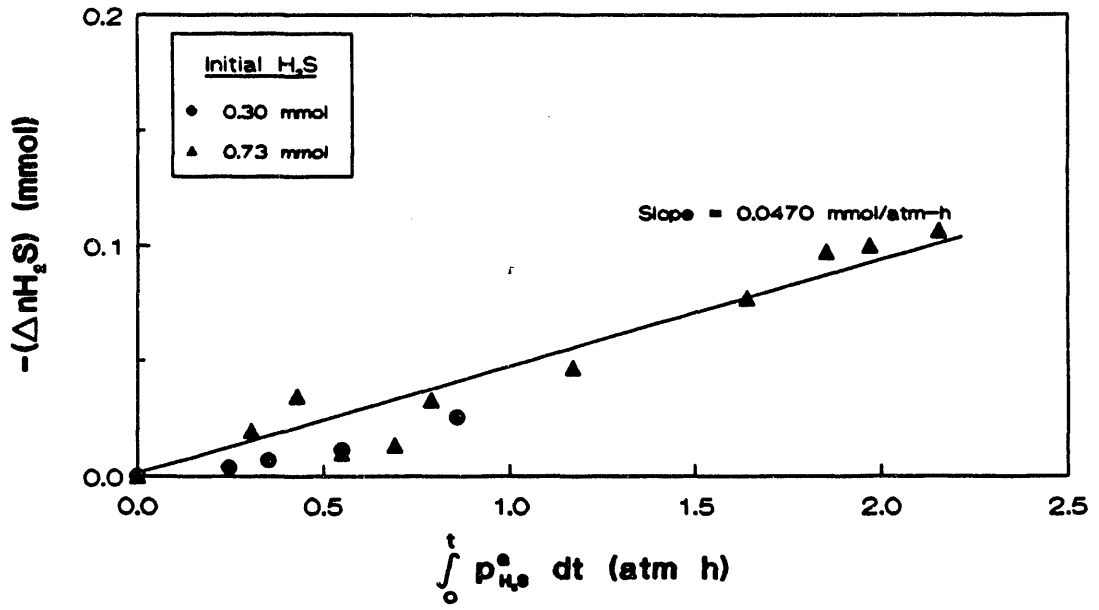

Figure 4.3. Determination of the first-order rate constant for H_2S disappearance into butyl rubber septa.

$$k = 1.06 \times 10^{12} e^{-22710/RT} \quad (4.3)$$

where k is the first order rate constant, sec^{-1};

R is the ideal gas constant, 1.987 cal/gmole°C; and

T is the absolute temperature, °K.

At 37°C, the rate constant is thus calculated as 0.37 h^{-1}.

C. thiosulfatophilum can utilize COS indirectly, by utilizing the H_2S produced by the chemical reaction in Equation (1.4). If this is a satisfactory process, it will eliminate the need for an additional organism (such as *Rhodospirillum rubrum* or *Peptostreptococcus productus*) for COS degradation.

Figures 4.4-4.9 show cell growth, gas phase COS uptake and gas phase production and uptake profiles for indirect COS utilization by *C. thiosulfatophilum*. Two experiments were performed: one with 0.2, 0.9 and 0.6 mmol of COS initially; and one with 0.3, 0.5 and 0.8 mmol of COS initially.

In examining the cell concentration profiles of Figures 4.4 and 4.5, it is seen that typical cell concentration profiles are obtained even though COS is utilized by an indirect route. It also appears that the lag phase is slightly larger for the highest initial COS levels.

Figures 4.6 and 4.7 present gas phase COS concentration profiles for the two experiments. Also shown in each figure are the results of an experiment using the highest COS level (0.6 mmol and 0.8 mmol, respectively) and no culture. As is noted in the two figures, the rate of disappearance of COS from the batch reactors, as determined from the slopes of the COS concentration profiles, is identical with and without culture regardless of the initial COS level. This result indicates that the rate limiting step in

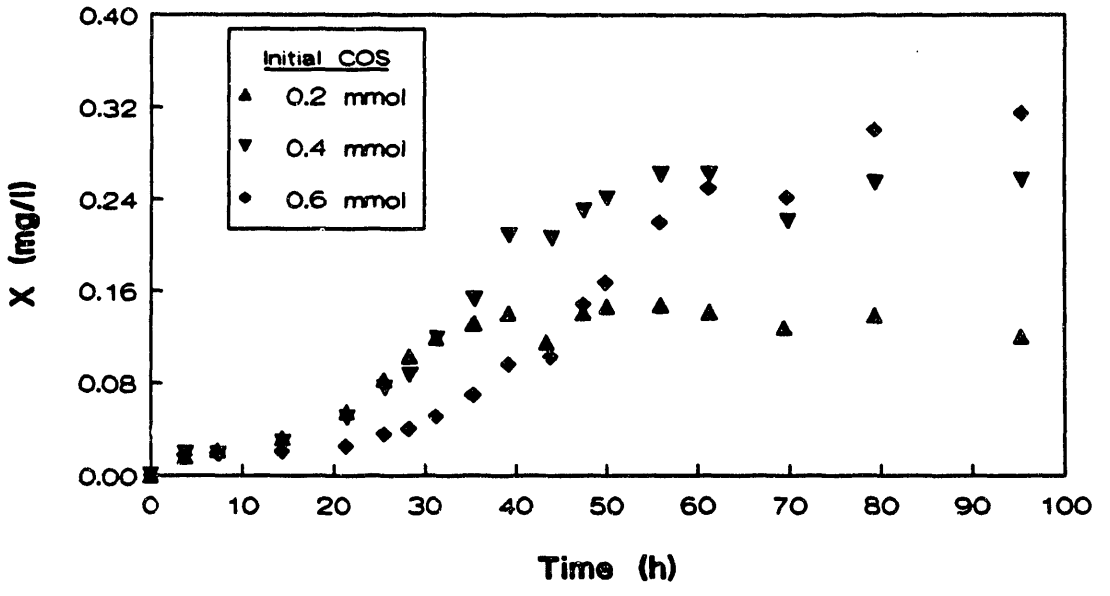

Figure 4.4. Cell concentration profiles for the indirect uptake of COS by *C. thiosulfatophilum* (Experiment 1).

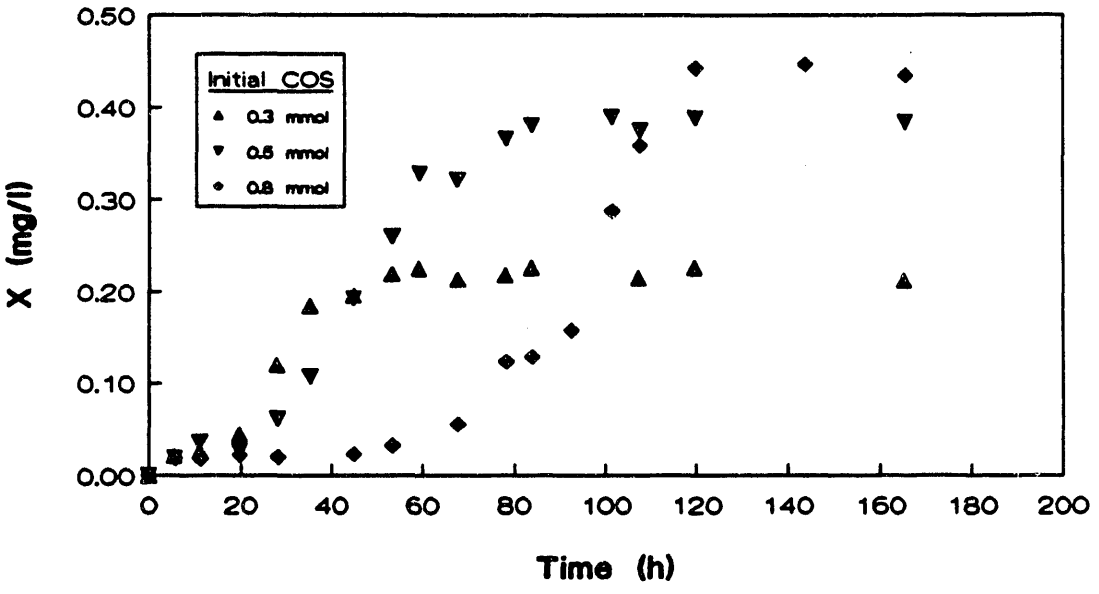

Figure 4.5. Cell concentration profiles for the indirect uptake of COS by *C. thiosulfatophilum* (Experiment 2).

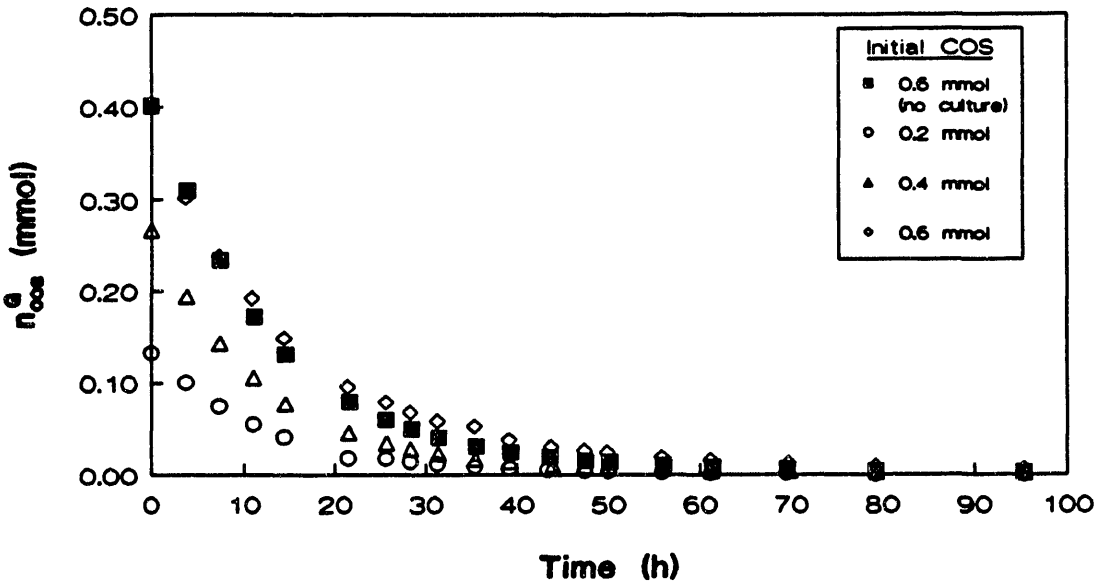

Figure 4.6. Gas phase COS uptake profile for *C. thiosulfatophilum* (Experiment 1).

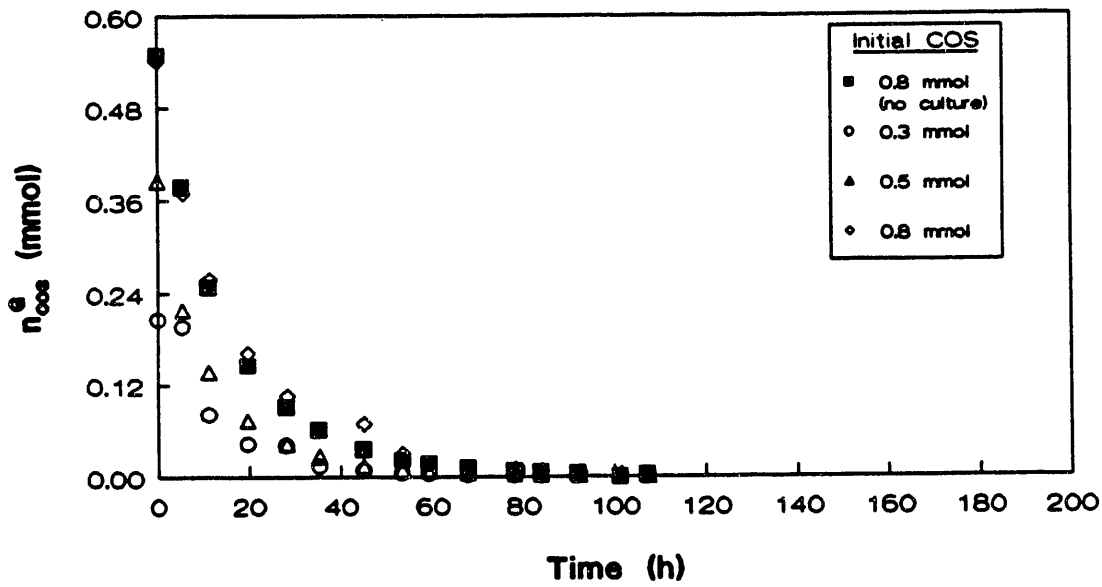

Figure 4.7. Gas phase COS uptake profile for *C. thiosulfatophilum* (Experiment 2).

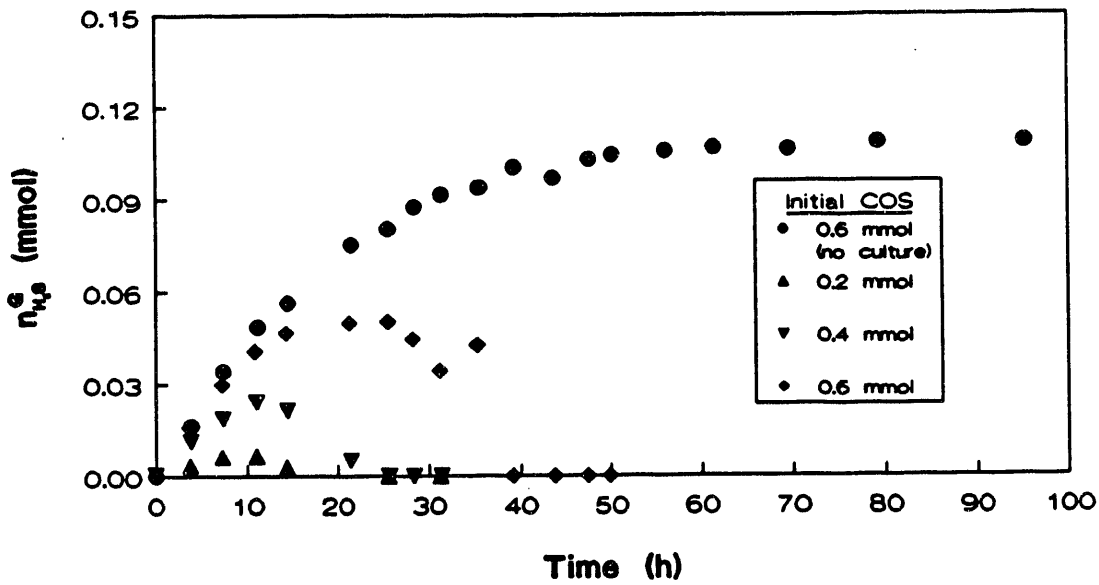

Figure 4.8. Gas phase H_2S production (from COS) and uptake profile by *C. thiosulfatophilum* (Experiment 1).

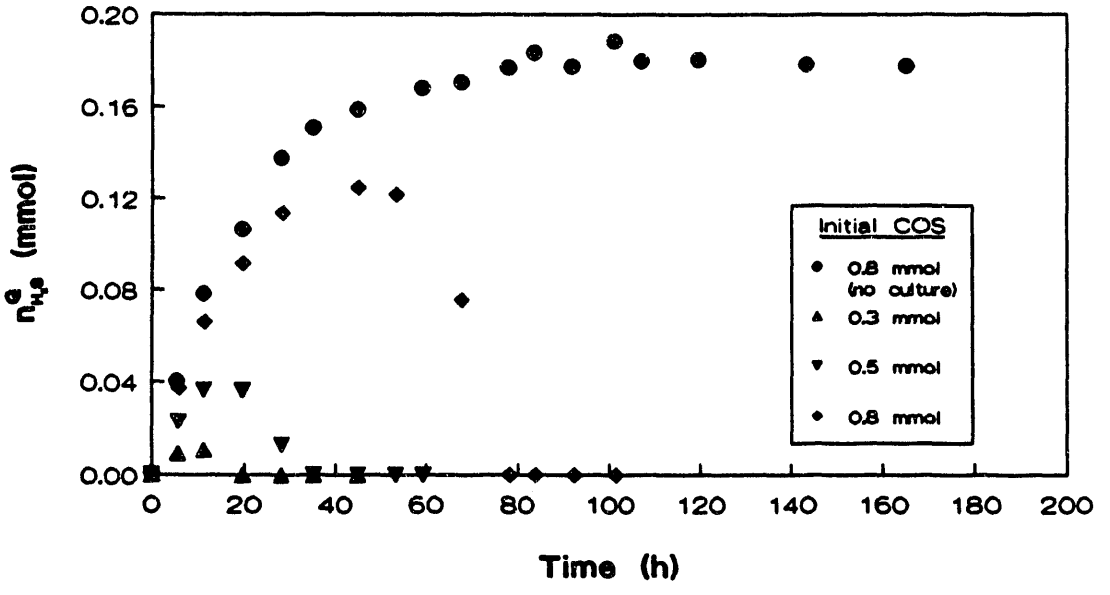

Figure 4.9. Gas phase H_2S production (from COS) and uptake profile by *C. thiosulfatophilum* (Experiment 2).

COS uptake is the reaction of COS with water by Equation (1.4). Thus, the actual uptake of COS does not depend upon the initial concentration of COS, at least until the initial COS level reaches very high inhibitory levels.

Figures 4.8 and 4.9 show gas phase H_2S production (by the chemical reaction) and uptake profiles for the two experiments for *C. thiosulfatophilum*. As in Figures 4.6 and 4.7, profiles without culture are also shown at the highest initial COS levels. As is noted in Figures 4.8 and 4.9, the profiles without culture showed the gradual accumulation of H_2S with time. The production of H_2S by Equation (1.4) is indeed a relatively slow reaction. As is noted in the experimental runs with culture, the H_2S produced by the chemical reaction was not immediately consumed by the culture. Consumption did not occur due to the low initial cell density. It should be remembered that H_2S is required for growth. There was no evidence that COS could be directly utilized by *C. thiosulfatophilum*. There is also some evidence to suggest that COS may even be inhibitory to the growth of the bacterium and its ability to utilize COS.

Figure 4.10 shows a plot of the increased total sulfur (COS (g), H_2S (g), total sulfide species) profiles for the data without culture in Figures 4.6-4.9. It is assumed in this plot that all COS in the liquid phase had been converted to H_2S. As is noted in the figure, one experiment showed essentially constant total sulfur, while the other experiment showed that the total sulfur content decreased slightly with time.

Figure 4.11 shows the same profile as in Figure 4.10 now corrected for H_2S disappearance into the stopper by the results of Figure 4.3. As is noted in Figure 4.11, now one set of data shows increasing total sulfur with time, while the other data set shows essentially constant total sulfur with time.

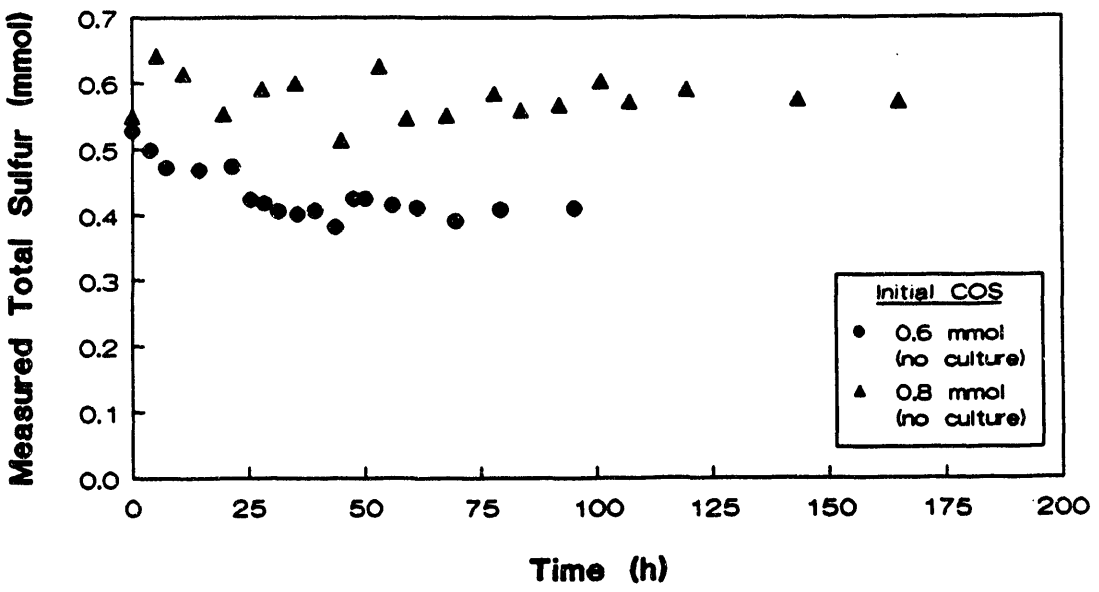

Figure 4.10. Measured total sulfur profile without culture of COS conversion to H_2S.

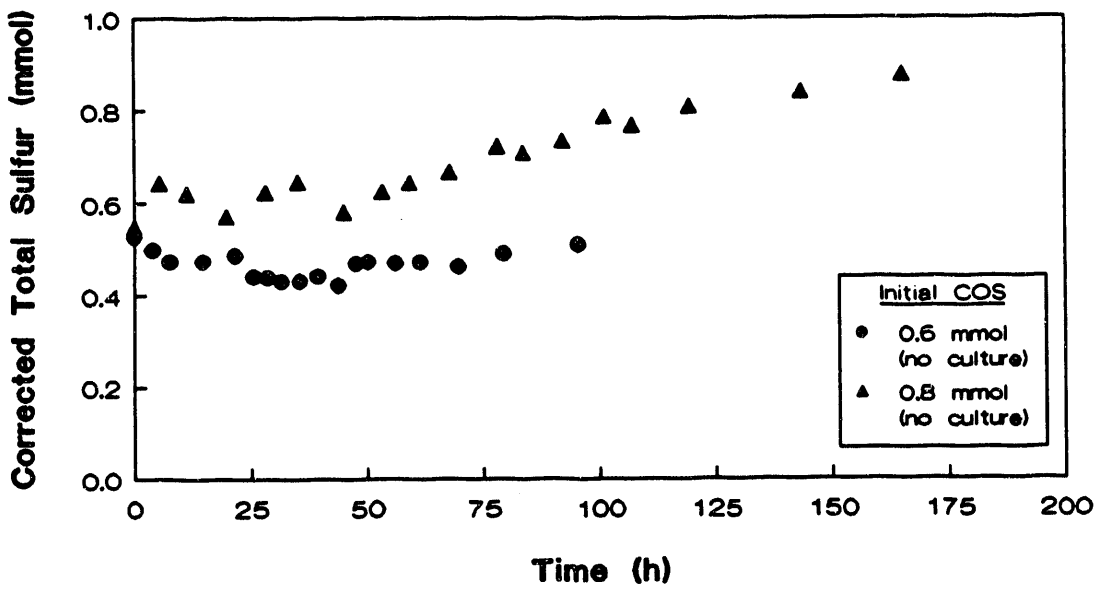

Figure 4.11. Measured total sulfur profile without culture for COS conversion to H_2S (corrected for H_2S disappearance into rubber stopper).

Obviously, sulfur is not always lost to the stoppers, thus complicating the correction for H_2S disappearance.

Figure 4.12 utilizes the same data to determine the actual experimental stoichiometry of Equation (1.4). According to Equation (1.4), a slope of 1.0 should result when H_2S production (corrected for disappearance into the stoppers) is plotted against COS consumption. As is noted in Figure 4.12, a slope of 0.94 mol/mol is attained, thereby verifying the stiochiometry of Equation (1.4).

The kinetics of the chemical reaction in Equation (1.4) may also be determined from the data of Figures 4.6-4.9. The rate of disappearance of COS from the gas and liquid phases may be written as:

$$- \frac{d}{dt} \left[n^G_{COS} + n^L_{COS} \right] = k_t \cdot C^L_{COS} \cdot V_L = k_t \cdot \frac{P_{COS}}{H} \cdot V_L \qquad (4.4)$$

Assuming that $k_t << K_La$, $P^L_{COS} = P^G_{COS}$ at equilibrium

Therefore,

$$- \frac{d}{dt} \left[\frac{P^G_{COS} \cdot V_G}{RT} + \frac{P^G_{COS} \cdot V_L}{H} \right] = k_t \frac{P^G_{COS}}{H} \cdot V_L \qquad (4.5)$$

Thus, a plot of $- \left[\frac{1}{V_L} \right] \frac{d}{dt} \left[P^G_{COS} \left(\left[\frac{H}{RT} \right] V_G + V_L \right) \right]$ as a function of P^G_{COS} should yield a straight line of slope k_t. In this plot,

$$\frac{H}{RT} = \frac{55.10}{0.08206 \cdot (273.15 + 30)} = 2.215 \text{ (dimensionless)}$$

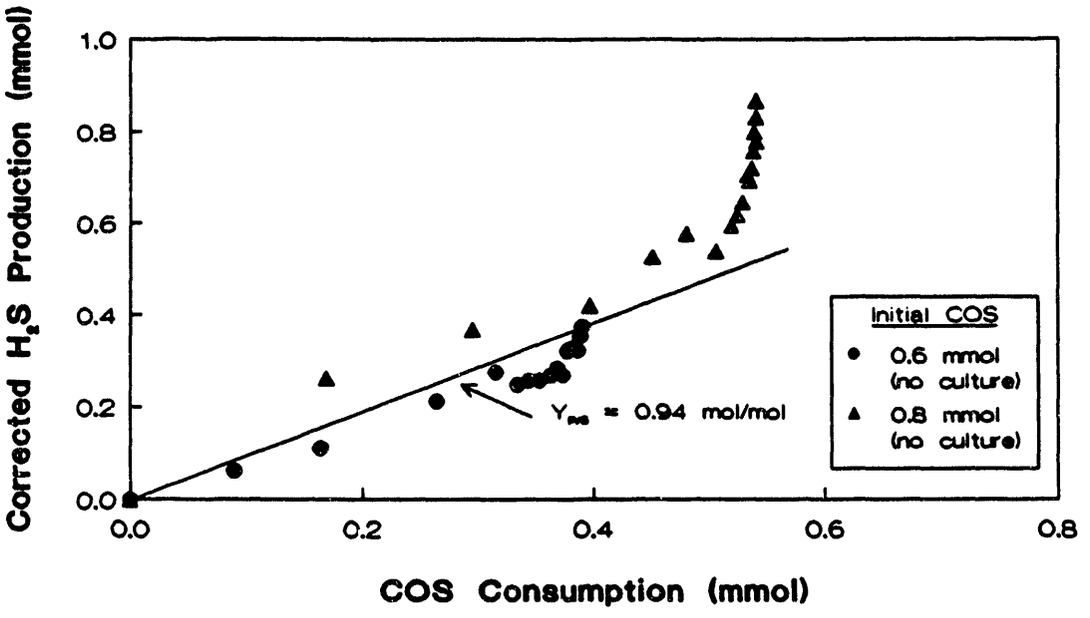

Figure 4.12. Deterimnation of stoichiometry for Equation 1.4.

As is noted, a fairly good correlation was obtained between the raw data and the predicted values obtained from the correlation. The specific growth rate asymptotically approached the maximum specific growth rate of 0.152 h^{-1} as predicted by the model.

In comparing the Monod equations for *C. thiosulfatophilum* and *R. rubrum*, it is seen that the maximum specific growth rate, μ_m, for *C. thiosulfatophilum* is 3 times the value for *R. rubrum* (0.152 h^{-1} versus 0.052 h^{-1}). In addition, the value for K_I for *C. thiosulfatophilum* was 2.5 times the value for *R. rubrum* (351 lux vs 140 lux). This latter result means that a 50% reduction in the maximum specific growth rate occurs at a much higher light intensity for *C. thiosulfatophilum* than *R. rubrum*.

A comparison of specific growth rates for the two bacteria as a function of light intensity is shown in Table 4.1. As expected, *C. thiosulfatophilum* consistently showed higher specific growth rates than *R. rubrum* at a given light intensity. This may occur because *C. thiosulfatophilum* utilizes both chemical energy (H_2S, S) and light energy to supply energy for growth, while *R. rubrum* utilizes light energy only as a source of energy for cell growth.

Such a plot is shown in Figure 4.13. As is noted, a rate constant of 0.243 h^{-1} is attained, which compares well with the values of 0.144 h^{-1} at 30°C or 0.339 h^{-1} at 37°C obtained by Thompson *et al.* (37). Smith (38) obtained a value of 0.25 h^{-1} under the exact same experimental conditions as the experiment in Figure 4.13.

4.4 Growth Kinetics for *C. thiosulfatophilum* Using Light as the Limiting Substrate

In determining growth kinetics for *C. thiosulfatophilum*, two batch experiments were conducted with a set of five reactors per experiment. Using natural grey light reduction filters, various incoming light intensities were achieved. The cell concentration (X) was obtained as a function of time and these cell concentration profiles are shown in Figure 4.14 for one of the experiments. As is noted in Figure 4.14, growth increased with increasing light intensity up to a light intensity of about 1000 lux. The initial specific growth rate for each reactor was estimated with increasing light intensity. The initial specific growth rate for each reactor was estimated as the slope of the line from a plot of ln(X) as a function of time, shown in Figure 4.15.

Using the values from Figure 4.15 and the relationship presented in Equation (3.16), the values for the parameters μ_m and K_I were found to be 0.152 h^{-1} and 351 lux, respectively. This indicates a maximum specific growth rate of 0.152 h^{-1} for the conditions employed and a 50% reduction of the maximum growth rate at a light intensity of 351 lux. In Figure 4.16, the initial specific growth rate is plotted as a function of light intensity. The curve in Figure 4.16 is obtained from the empirical model

$$\mu = \frac{0.152\ I_o}{351 + I_o} \qquad (4.6)$$

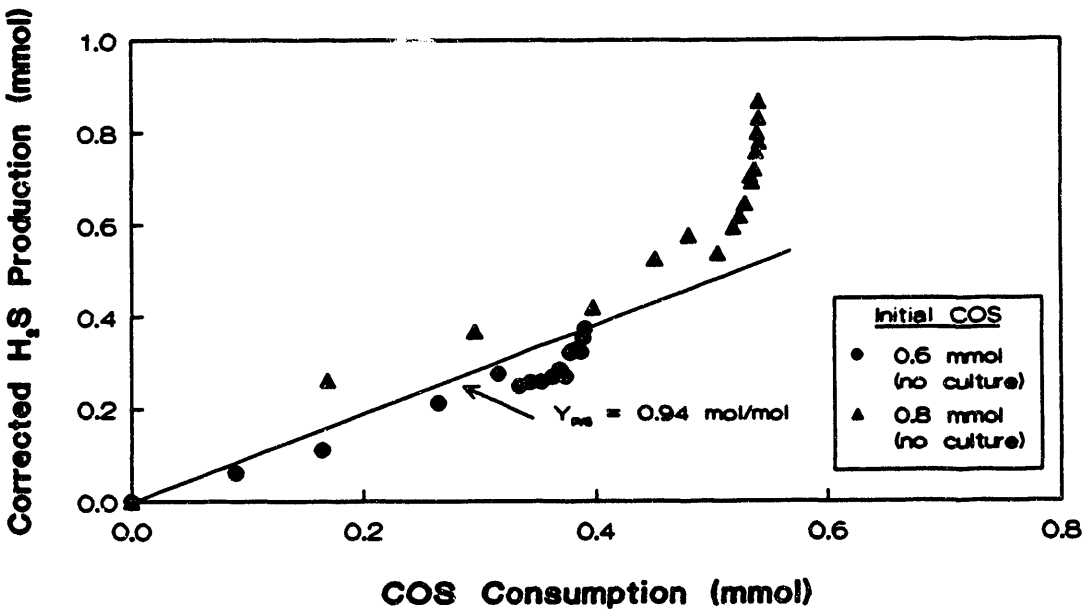

Figure 4.13. Deterimnation of the first order reaction rate constant for the reaction: $COS + H_2O - H_2S + CO_2$.

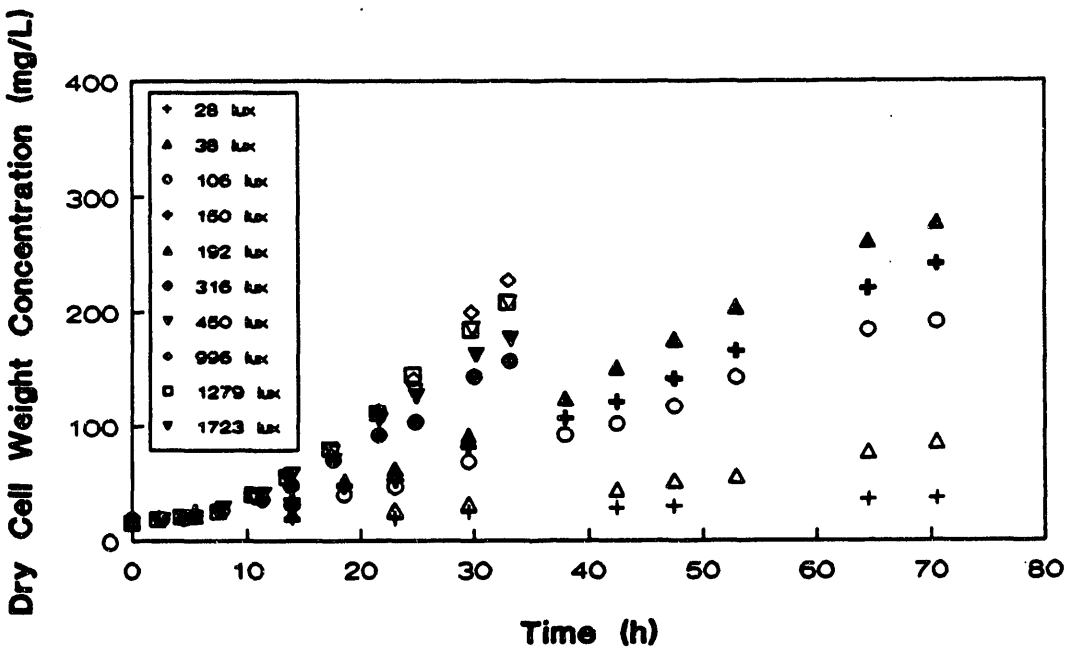

Figure 4.14. Cell concentration profiles for *C. thiosulfatophilum* as a function of incoming light intensity.

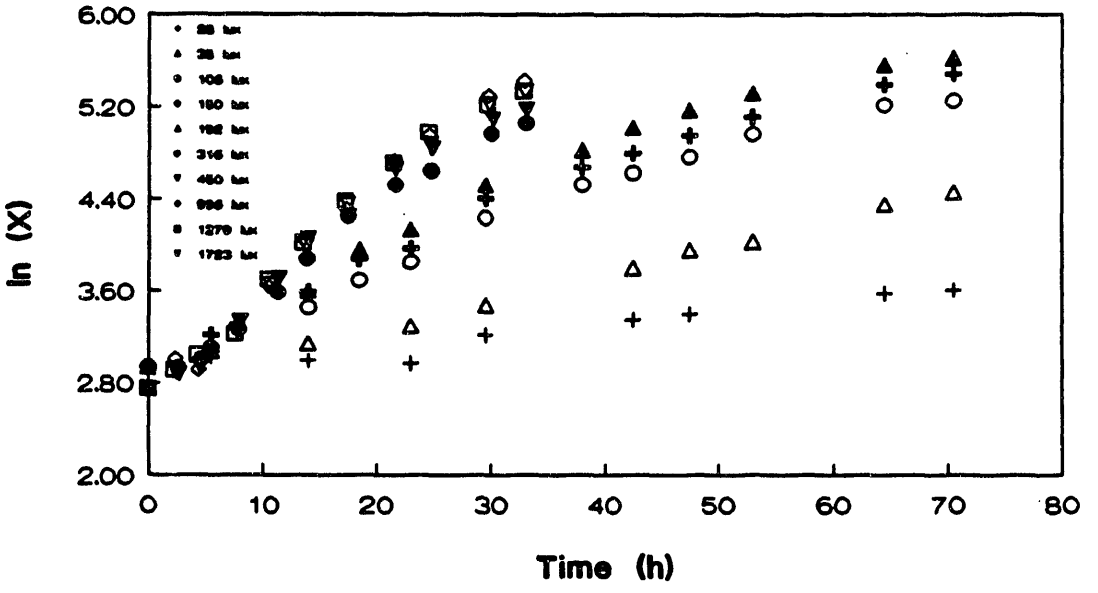

Figure 4.15. Determination of initial specific growth rates for *C. thiosulfatophilum* at various light intensities.

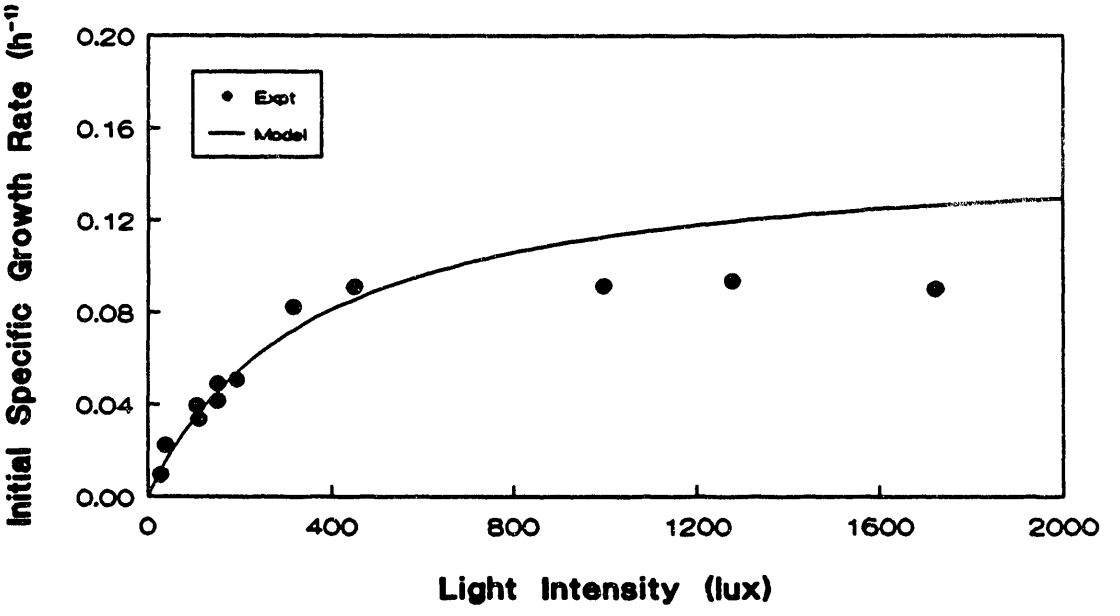

Figure 4.16. Comparison of monod model with experimental data for the light intensity study with *C. thiosulfatophilum.*

Table 4.1

Calculated Specific Growth Rates for *R. rubrum* and *C. thiosulfatophilum* from Monod Equations

Light Intensity (lux)	Specific Growth Rate, μ (h^{-1})	
	R. rubrum	C. thiosulfatophilum
50	0.014	0.019
100	0.022	0.034
200	0.031	0.055
300	0.035	0.070
500	0.041	0.089
700	0.043	0.101
1000	0.046	0.113
1500	0.048	0.123

5.0 CONCLUSIONS

Mass transfer and kinetic studies were carried out for the *Rhodospirillum rubrum* and *Chlorobium thiosulfatophilum* bacterial systems. *R. rubrum* is a photosynthetic anaerobic bacterium which catalyzes the biological water gas shift reaction:

$$CO + H_2O \rightarrow CO_2 + H_2 \qquad (1.3)$$

C. thiosulfatophilum is also a photosynthetic anaerobic bacteria, and converts H_2S and COS to elemental sulfur.

Batch studies with *R. rubrum* have demonstrated that CO utilization can be modeled by the equation:

$$q = \frac{0.055\ P_L^*}{0.45 + P_L^* + \left(P_L^*\right)^2/0.106} \qquad (3.6)$$

A similar equation was found for CO utilization in continuous (CSTR) culture:

$$q = \frac{0.0146\ P_{CO}^*}{0.0053 + P_{CO}^*}\left(1 - \frac{P_{CO}^*}{0.68}\right) \qquad (3.22)$$

The growth of *R. rubrum* in terms of incoming light intensity is given by the equation:

$$\mu = \frac{0.052\ I_o}{140 + I_o} \qquad (3.17)$$

The growth of *R. rubrum* may be satisfactorily carried out at 25° and 30°C, while CO uptake and thus the conversion of CO best occurs at temperatures of either 30°, 32° or 34°C.

The rate of conversion of COs and H_2O to CO_2 and H_2S may be modeled by a first order rate expression. The rate constant at 30°C was found to be 0.243 h^{-1}. The growth of *C. thiosulfatophilum* may be modeled in terms of incoming light intensity using a Monod equation:

$$\mu = \frac{0.152\ I_o}{351 + I_o} \qquad (4.6)$$

Comparisons of the growth of *R. rubrum* and *C. thiosulfatophilum* shows that the specific growth rate of *C. thiosulfatophilum* is much higher at a given light intensity.

6.0 NOMENCLATURE

C	concentration	mol/L
G	volumetric gas flow rate	L/h
H	Henry's law constant for CO	L atm/mol
I	Light intensity	lux
K_I, K_p	Monod saturation constant	lux
K_La	overall mass-transfer coefficient	h^{-1}
n	number of moles	mol
P	partial pressure	atm
q	specific CO uptake rate by cells	mol/g h
r	volumetric CO mass-transfer/uptake rate	mol/h L
R	ideal gas law constant	L atm/mol °K
t	time	h
T	absolute temperature	°K
V	volume	L
W	Substrate inhibition constant	atm
X	cell concentration	g/L
z	distance	
ϵ	extinction coefficient	
μ	specific growth rate	h^{-1}

Superscripts and Subscripts

*	equilibrium value
Ar	argon, inert tracer gas
CO	carbon monoxide
G	gas phase

7.0 LITERATURE CITED

1. McCullough, G.R. S.C.Roberts, and M.J. Van der Burgt, (1982), *Energy Prog.* 2, 69.

2. Koh, W.K. (1982), *Hydro. Proc.* 61(6), 85.

3. Eagen, C.A., Jr., and R.C. Wessenhott, (1981), *Energy Prog.* 1, 104.

4. Kaplan, L.J. (1982), *Chem. Engr.* 89(6), 64.

5. Richardson, J.T. (1973), *Hydro. Proc.* 52(12), 99.

6. Jockel, H. and B.E. Triesbskorn, (1973), *Hydro. Proc.* 52(1), 93.

7. Courty, D. and P. Chaumette, (1987), *Energy Prog.* 7, 23.

8. Schreiner, M., (1978), "Research Guidance Studies to Assess GAsoline from Coal by Methanol-to-Gasoline and Sasol-Type Fischer-Tropsch Technologies," Report No. FE-2447-13, U. S. Department of Energy, Washington, D. C.

9. Simbeck, D.R., R.L. Dickerson, and A.J. Moll, (1982), *Energy Prog.*, 2.1, 42.

10. Fleming, D.K. and H.S. Primack, (1976), "Purification Processes for Coal Gasification," presented at the 18th National Meeting of the American Institute of Chemical Engineers, Kansas City.

11. Probstein, R.F., and R.E. Hicks (1982), *Synthetic Fuels*,, McGraw-Hill, New York.

12. Barik, S., R. E. Corder, E.C. Clausen, and J.L. Gaddy, (1987), *Energy Prog.* 7, 157.

13. Vega, J.L., K.T. Klasson, D.E. Kimmel, C.W. Ko, E.C. Clausen, and J. L. Gaddy, (1989), "Advanced Studies of the Biological Conversion of Coal Synthesis Gas to Methane. Topical Report on Task 4. Sulfur Toxicity," U.S. Department of Energy, Morgantown Energy Technology Center, Contract No. DE-AC-21-86MC23281.

14. Vega, J.L., G.A. Antorrena, E.C. Clausen, and J.L. Gaddy (1989), "Bioreactor Design for Gaseous Substrate Fermentations," *Proceedings of the IGT Symposium on Gas, Oil and Coal Biotechnology.*

15. Klasson, K.T., J.P. Cowger, C.W. Ko, J.L. Vega, E.C. Clausen, and J.L.Gaddy (1990), "Methane Production from Synthesis Gas Using a Mixed Culture of *R. rubrum, M. Barkeri* and *M. formicicum*" to appear in *Applied Biochemistry and Biotechnology.*

7.0 Literature Cited (continued)

16. Cork, D.J. and S. Ma (1982), *Biotechnol. and Bioeng. Symposium Series,*, 12, 285.

17. Cork D.J., R. Garunas, and A. Sajjad (1983), *Appl. Environ. Microbiol.* 45, 913.

18. Sublette, K.L. and N.D. Sylvester (1987), *Biotechnol. and Bioeng.*, 29, 753.

19. Sublette, K.L. (1987), *Biotechnol. Bioengr.*, 29, 690.

20. McInerney, M.J., M.P. Bryant, and N. Pfennig (1979), "Anaerobic Bacterium that Degrades Fatty Acids in Syntrophic Association with Methanogens," *Arch. Microbiol.*, 122, 129.

21. Genthner, B.R.S., M.P. Davis, and M.P. Bryant (1981), "Features of Rumen and Sewage Sludge Strains of *Eubacterium limosum*, a Methanol- and H_2-CO_2-Utilizing Species," *Appl. Environ. Microbiol.*, 42, 12.

22. Bailey, J.E. and D.F. Ollis (1986), *Biochemical Engineeing Fundamentals*, 2nd ed., McGraw-Hill, New York, p 457.

23. Monod, J (1949), "The Growth of Bacterial Cultures," *Annual Reviews of Microbiology*, 3, 371.

24. Andrews, J.F. (1968), "A Mathematical Model for the Continuous Culture of Microorganisms Utilizing Inhibitory Substrates," *Biotechnol. Bioeng.*, 10, 707.

25. Vega, J.L., E.C. Clausen, and J.L. Gaddy (1989), "Study of Gaseous Substrate Fermentations: Carbon Monoxide Conversion to Acetate, 1. Batch Culture," *Biotechnol. Bioeng.*, 34 774.

26. Foust, A.S., L.A. Wenzel, C.W. Clump, L. Mous, and L.B. Andersen (1960), in *Principles of Unit Operations*, John Wiley & Sons, New York, p. 552.

27. Vignais, P.M., A. Colbeau, J.C. Willison, and Y. Jouanneau (1985), "Hydrogenase, Nitrogenase, and Hydrogen Metabolism in the Photosynthetic Bacteria," in *Advances in Microbial Physiology*, Vol. 26, A.H. Rose and D.W. Tempest, eds., Academic Press, London, p. 155.

28. Bott, M., B. Eikmanns, and R.K. Thauer (1986), "Coupling of Carbon Monoxide Oxidation to CO_2 and H_2 with the Phophorylation of ADP in Acetate-Grown *Methanosarcina barkeri*," *Eur. J. Biochem.*, 159, 393.

29. Sada, E., S. Katoh, A. Kheirolomoo, and H. Yokoi (1989), *J. Ferment. Bioeng.*, 67(2), 315.

7.0 Literature Cited (continued)

30. Philips, E.J. and A. Mitsui (1983), *Appl. Environ. Microbiol.*, 45(4), 1212.

31. Rabe, A.E. and R.J. Benoit, (1962), *Biotechnol. Bioeng.*, 4, 377.

32. Erickson, L.E., C.E. Curless, and H.Y.Lee (1987), *Ann. N.Y. Acad. of Sci.*, 506, 308.

33. Göbel, F. (1978), in *The Photosynthetic Bacteria*, R.K. Clayton and W.R. Sistrom, eds, Plenum Press, New York, p. 907.

34. Holt, S.C. and A.G. Marr (1965), *J. Bacteriol.*, 89(5), 1421.

35. Cohen-Bazire, G. and W.R. Sistrom (1966), in *The Chlorophylls*, L.P. Vernon and G.R. Seedy, eds., Academic Press, New York, p. 313.

36. Bailey, J.E. and D.F. Ollis (1977), *Biochemical Engineering Fundamentals*, 2nd ed., McGraw-Hill, New York, p. 282.

37. Thompson, H.W., C.F. Kearton and S.A. Lamb (1935), "The Kinetics of the Reaction Between Carbonyl Sulphide and Water," *J. Chemical Society*, Part II.

38. Smith, K.D. (1990), "The Biological Removal of Carbonyl Sulfide from Coal Derived Synthesis Gas Streams," M.S. Thesis, University of Arkansas.

END

DATE FILMED

4/16/93